

Be stars and binaries in the field of the SMC open cluster NGC330 with VLT-FLAMES

C. Martayan¹, M. Floquet¹, A.M. Hubert¹, J. Gutiérrez-Soto^{1,2}, J. Fabregat², C. Neiner¹, and M. Mekkas¹

¹ GEPI, Observatoire de Paris, CNRS, Université Paris Diderot; place Jules Janssen 92195 Meudon Cedex, France

² Observatorio Astronómico de Valencia, edifici Instituts d'investigació, Poligon la Coma, 46980 Paterna Valencia, Spain

Received / Accepted

ABSTRACT

Aims. Observations of hot stars belonging to the young cluster SMC-NGC330 and its surrounding region were obtained with the VLT-GIRAFFE facilities in MEDUSA mode. We investigated the B and Be star properties and proportions in this environment of low metallicity. We also searched for rapid variability in Be stars using photometric databases.

Methods. With spectroscopic measurements we characterized the emission and properties of Be stars. By cross-correlation with photometric databases such as MACHO and OGLE, we searched for binaries in our sample of hot stars, as well as for short-term variability in Be stars.

Results. We report on the global characteristics of the Be star sample (131 objects). We find that the proportion of early Be stars with a large equivalent width of the H α emission line is higher in the SMC than in the LMC and MW. We find a slight increase in the proportion of Be stars compared to B-type stars with decreasing metallicity. We also discovered spectroscopic and photometric binaries, and for the latter we give their orbital period. We identify 13 Be stars with short-term variability. We determine their period(s) and find that 9 Be stars are multiperiodic.

Key words. Stars: early-type – Stars: emission-line, Be – Galaxies: Magellanic Clouds – Stars: binaries: spectroscopic – Stars: binaries: eclipsing – Stars: oscillations

1. Introduction

The Magellanic Clouds (MC), which contain a huge number of early-type stars, are particularly appropriate to investigate the effect of low metallicity on the B and Be stars populations, comparatively to the ones in the Milky Way (MW). The FLAMES-GIRAFFE instrumentation (Pasquini et al. 2002) installed at the VLT allowed us to obtain significant samples of B and Be stars spectra in the Large and Small Magellanic Clouds (LMC and SMC) which are needed to achieve our goal. In Martayan et al. (2006c), we presented an overview of spectroscopic results for 176 early-type stars observed in the field of the LMC open cluster NGC2004. In Martayan et al. (2006b) and Martayan et al. (2007b) (hereafter Papers I and II) we searched for the effects of metallicity in the LMC and SMC, respectively. We showed that the lower the metallicity, the higher the rotational velocities. These observational results support theoretical predictions by Meynet & Maeder (2000, 2002) and Maeder & Meynet (2001) for massive stars. Therefore the percentage of Be stars seems to be higher in lower metallicity environments such as the SMC ($Z < 0.001$). In this fourth paper we present an overview of spectroscopic results for 346 early-type stars observed in the field of the SMC open cluster NGC330 with VLT-FLAMES. Note that the determination of their fundamental parameters (T_{eff} , $\log g$, $V \sin i$, and RV) has already been reported in Paper II. We also search for pulsators among

our Be stars sample through an analysis of their MACHO¹ data. Theoretically, the pulsational instability of hot stars has a great dependence on metallicity. Pamyatnykh (1999) showed that the instability strip for β Cephei and Slow Pulsating B stars (SPB) vanishes at $Z < 0.01$ and $Z < 0.006$, respectively. Thus, Be stars, which show the same pulsational characteristics as those of classical B-type pulsators (e.g. Neiner et al. 2005; Walker et al. 2005a,b) in the MW, are among the best objects in the SMC to test their theoretical predictions.

In the present paper, the observations and the reduction process are described in Sect. 2. In Sect. 3 we present the characteristics of the H α emission line and the proportion of Be stars in the field as well as in clusters and OB associations. We perform a comparison with Be stars in the MW (Sect. 3.2.3). In Sect. 4 we describe the variability detected in our Be stars sample thanks to an investigation of the MACHO and OGLE databases (Szymanski 2005). We report on the discovery of spectroscopic and photometric binaries (Sect. 4.1) and the identification of multi-periods in the light curves of several objects (Sect. 4.2) which pleads in favour of pulsations. We discuss the impact of metallicity on the proportion of Be stars and the presence of pulsations in Sect. 5. Finally, we give a detailed study of 3 peculiar emission line objects that are not classical Be stars (Appendix A), of binary systems (Appendix B), and of short-term periodic Be stars (Appendix C).

Send offprint requests to: C. Martayan

Correspondence to: christophe.martayan@obspm.fr

¹ <http://www.macho.mcmaster.ca/>

2. Observations

Spectra of a significant sample of the B star population in the young cluster SMC NGC330 and its surrounding field have been obtained with the ESO VLT-FLAMES facilities, as part of the Guaranteed Time Observation programs of the Paris Observatory (P.I.: F. Hammer). The multi-fibre spectrograph VLT-FLAMES has been used in MEDUSA mode (132 fibres) at medium resolution.

As shown in Paper I and II the use of the setup LR02 (396.4–456.7 nm, hereafter blue spectra) is adequate for the determination of fundamental parameters, while the LR06 setup (643.8–718.4 nm, hereafter red spectra) is used to identify Be stars and to study the $H\alpha$ emission line characteristics. The spectral resolution is 6400 for LR02 and 8600 for LR06. The respective instrumental broadenings are $\simeq 50 \text{ km s}^{-1}$ and 35 km s^{-1} . Observations (ESO runs 72.D-0245A and 72.D-0245C) were carried out on October 21, 22 and 23, 2003 (blue and red spectra) and on September 9 (blue spectra) and 10 (red spectra), 2004. The observational seeing ranged from 0.4 to 2".

The observed fields are centred at $\alpha(2000) = 00^{\text{h}} 55^{\text{m}} 15^{\text{s}}$ and $\delta(2000) = -72^{\circ} 20' 00''$ for the observations of 2003 and at $\alpha(2000) = 00^{\text{h}} 55^{\text{m}} 25^{\text{s}}$ and $\delta(2000) = -72^{\circ} 23' 30''$ for the run of 2004. Besides the young cluster NGC330, these fields contain several high-density groups of stars. The position of all our stellar and sky fibre targets is plotted in Fig. 1 (online).

A sample of 346 stars among the 5370 B-type star candidates located in the selected fields has been observed during the two observing runs (see Paper II, Sect. 2). It contains 131 Be stars, 202 B-type stars, 4 O-type stars, 6 A-type stars, and 3 other types of stars, which are discussed in this paper.

The data reduction was performed as described in Paper I and II. The S/N ratio of spectra obtained in the blue region varies from ~ 15 for the fainter objects to ~ 135 for the brighter ones (see Table 3 in Paper II).

3. Results

After subtraction of the sky line contribution, it appeared that more than 80% of the 346 stars are contaminated by nebular lines. This contamination is particularly detectable in the $H\alpha$ line. Depending of the intensity level of the nebular $H\alpha$ line, a weak nebular contribution can also be detected in forbidden lines of [NII] at 6548 and 6583 Å and [SII] at 6717 and 6731 Å in the LR06 setup. When the nebular $H\alpha$ line is strong, the $H\gamma$ and $H\delta$ line profiles are also affected by a nebular component. With the same technique as the one used to identify stars with the Be phenomenon in the LMC (Martayan et al. 2006c), we tried to disentangle the circumstellar line emission (CS) component from emission produced by the nebular line in polluted spectra.

3.1. Stellar and nebular radial velocities

For each star, the radial velocity (RV) of nebular lines ($H\alpha$, [NII], and [SII]) has been measured and compared to the stellar RV. The mean accuracy is $\pm 10 \text{ km s}^{-1}$. The statistical distribution of stellar and nebular RVs is mono-modal with a maximum at $+155 \text{ km s}^{-1}$ and $+165 \text{ km s}^{-1}$, respectively. The RV difference between stellar and nebular lines

peaks around -10 km s^{-1} and does not seem to indicate any clear link between stars and the structures giving rise to the nebular lines. However, due to the weak difference between the stellar and nebular RVs, it has not been easy to correctly estimate the nebularity contribution for Be stars which present a single-peaked $H\alpha$ emission line profile in their spectrum.

3.2. Be stars

Our sample contains 131 Be stars (see Table 1): 41 known Be stars including 39 ones from Keller et al. (1999) and 2 others from Grebel et al. (1992), and 90 Be stars discovered in Paper II (see Table 3 therein). Note that among this second group of Be stars, 28 ones are suspected to be emission line stars from a slit-less ESO-WFI survey (Martayan et al. 2006a).

3.2.1. Emission-line characteristics

The equivalent width (EW), maximum intensity (I_{max} for a single peak, and $I(V)$ and $I(R)$ for the violet and red peaks respectively in a double-peak emission), and the Full Width at Half Maximum (FWHM) of the circumstellar $H\alpha$ emission measured for each Be star are given in Table 1. The FWHM of the CS $H\alpha$ emission line ranges from 146 to 622 km s^{-1} . The telluric lines as well as the nebular lines are resolved and the FWHM of the $H\alpha$ nebular line is $\sim 60 \text{ km s}^{-1}$.

Not correcting for the nebular $H\alpha$ emission line contributes to overestimate I_{max} and underestimate the FWHM of the CS emission line. To a lesser degree it also leads to overestimate of $\text{EW}\alpha$. We thus determined and subtracted this contribution from the $H\alpha$ emission line profile. As in Martayan et al. (2006c), we used the nebular ratio $[\text{SII}]/H\alpha$ to estimate the nebular contribution in the CS $H\alpha$ line in Be star spectra. From the fibres located on sky positions (without stars in the background) we derived a mean intensity ratio $[\text{SII}]/H\alpha = 0.2 \pm 0.1$. The intensity and RV of the [SII] 6717 line can be measured in each Be star spectrum, if the line is present, and we assumed that the nebular line ratio $[\text{SII}]/H\alpha$ is the same for sky and star spectra. Consequently, we can generally state whether the $H\alpha$ CS emission is single, double or affected by these narrow absorption core of circumstellar origin.

Since we used the mean intensity ratio $[\text{SII}]/H\alpha$, the nebular contribution can be underestimated locally in some cases, which may lead to an overestimate of the number of Be stars with a single-peaked $H\alpha$, even more so because the RV of the nebular line is close to the stellar RV. Moreover, the lowest value of the V and R emission peak separation that can be measured is about 70–80 km s^{-1} . This limitation is chiefly found in Be stars with a low or moderate $V \sin i$ and a large EW in $H\alpha$.

Early Be stars, which represent the quasi-totality of our sample, show a CS emission contribution in the $H\gamma$ line profile when $\text{EW}\alpha$ is $\geq 15 \text{ Å}$, and in the $H\delta$ line profile when $\text{EW}\alpha$ is $\geq 30\text{--}40 \text{ Å}$. The detection limit depends on the S/N value. Fe II emission lines are often detected, however some spectra are too noisy to investigate their presence even if $\text{EW}\alpha$ is large.

The $H\gamma$ and $H\delta$ CS emission contribution is double-peaked except for Be stars with a low $V \sin i$ and a large

EW α . From Table 1, we find that the H α emission line is single-peaked for 60 objects after correction of the nebular contribution, and double-peaked for 71 objects. Moreover, about 30% of Be stars show an asymmetric or double emission H α profile with V/R or R/V ≥ 1.05 , consistent with the percentage in the MW (Hummel et al. 2001). Shell features observed in H lines and very often in metallic lines, are present in 22 Be stars.

3.2.2. Envelopes of Be stars

We examine the EW α distribution of the H α emission line for Be stars in the SMC and we search for correlations between $V\sin i$, FWHM α , EW α and ΔRV_{peaks} (the peak separation). Then, we compare them to the ones in the LMC and MW, respectively.

To study the EW α distribution we only consider Be stars in the MW with spectral types ranging from B0 to B4, in order to compare homogeneous samples, since the quasi-totality of Be stars we observed in the SMC and LMC are early-type B stars. Spectral types for Be stars in the SMC are taken from Paper II, as well as their $V\sin i$ obtained by fitting the observed spectra by theoretical spectra. For Be stars in the LMC we use data (EW α , spectral types and $V\sin i$) reported in Paper I, and for Be stars in the MW the ones summarized in Dachs et al. (1992), Andrillat & Fehrenbach (1982) and Andrillat (1983).

The EW α distributions for the SMC, LMC and MW are shown in Fig. 2. The rate of early Be stars with large EW α (>20 Å) is higher in the SMC than in the LMC and MW: 74% in the SMC to be compared with 62% in the LMC and 50% in the MW. Note that the shape of the distribution of EW is different in the SMC and peaks around -30 to -40 Å. It remains the same when we subtract the Be stars selected from the WFI survey (Martayan et al. 2006a).

We also examine the FWHM α distribution for Be stars in the SMC versus $V\sin i$. We obtain a linear correlation slightly different for stars with weak and strong EW α . As in the MW (e.g. Dachs et al. 1992), FWHM α at given EW α of emission increase as $V\sin i$. However, points corresponding to Be stars with an asymmetric H α emission line profile or with a V/R ratio $\neq 1$ are scattered in the graph. For more clarity we thus focus our study on Be stars with a symmetric single and double-peaked H α line profile and with EW $\alpha > 20$ Å. In Fig. 3 we plot the linear regressions for this sample in the SMC and its counterpart in MW.

From Figs. 2 and 3 we can conclude that on average Be stars in the SMC display lower FWHM α and larger EW α than their counterparts in the MW and the LMC. In the frame of a differentially rotating Keplerian disk model in which there is a direct relation between EW α and the radius of the emitting disk expressed in stellar units (Dachs et al. 1992; Grundstrom & Gies 2006) our result supports larger disk radii in the SMC compared to the MW and the LMC.

We find a correlation between $(\Delta RV_{\text{peaks}})/(2V\sin i)$ and EW α , as found for Galactic Be stars by Dachs et al. (1986) and Hanuschik et al. (1988), and refined by Zamanov et al. (2001), and for the LMC by Martayan et al. (2006a). This provides evidence for a rotationally supported CS envelope, as confirmed with the VLTI by Meilland et al. (2007) for the Galactic Be star α Arae.

Taking into account the fact that the dispersion of points

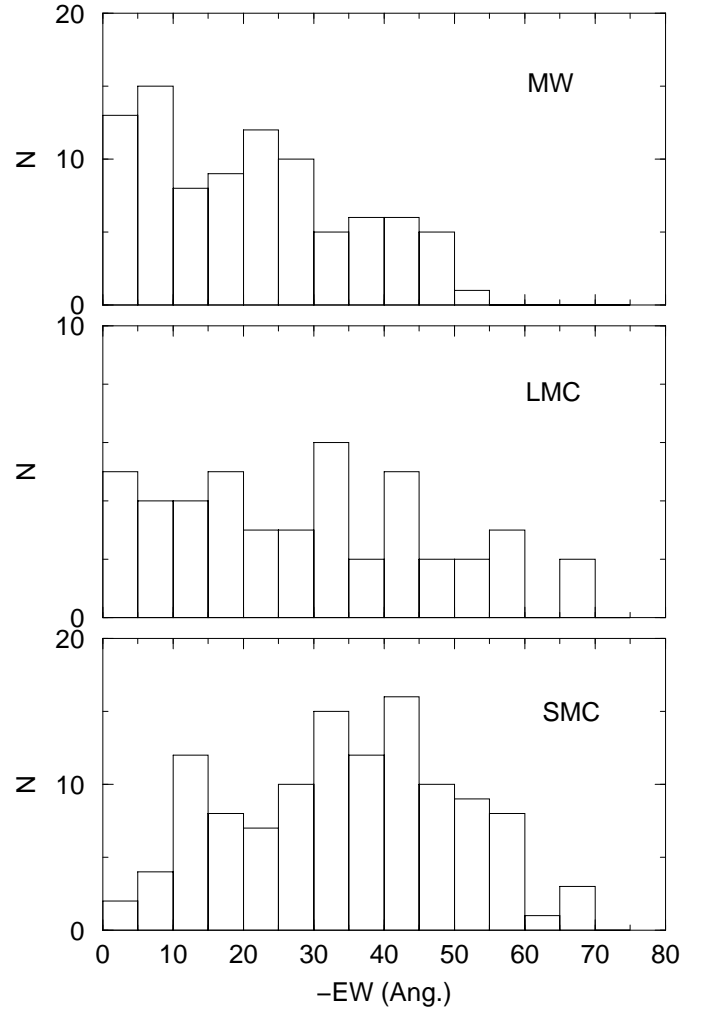


Fig. 2. Distributions of Be stars versus the EW of the H α emission line. Top: in the MW from Dachs et al. (1992), Andrillat & Fehrenbach (1982) and Andrillat (1983); middle: in the LMC from Paper I; bottom: in the SMC (this study).

for Galactic Be stars is similar to that for SMC Be stars (see Fig. 2a of Zamanov et al. 2001), the average slope of the peak separation versus the equivalent widths of Galactic Be stars determined by Zamanov et al. (2001) is comparable to ours in the SMC (see Fig. 4).

Note that as in the LMC, the SMC Be stars with a shell (triangles in Fig. 4) are located in the right part of the diagram, above the mean correlation. The increase of the peak separation in those objects is an opacity effect (see eq.(7) in Hanuschik et al. 1988). It indicates that SMC Be stars in shell phases have denser disks than stars without shell.

In addition to these distributions and graphs, we find the expected correlation between the intensity and the equivalent widths of the H α emission line for Be stars in the LMC and SMC.

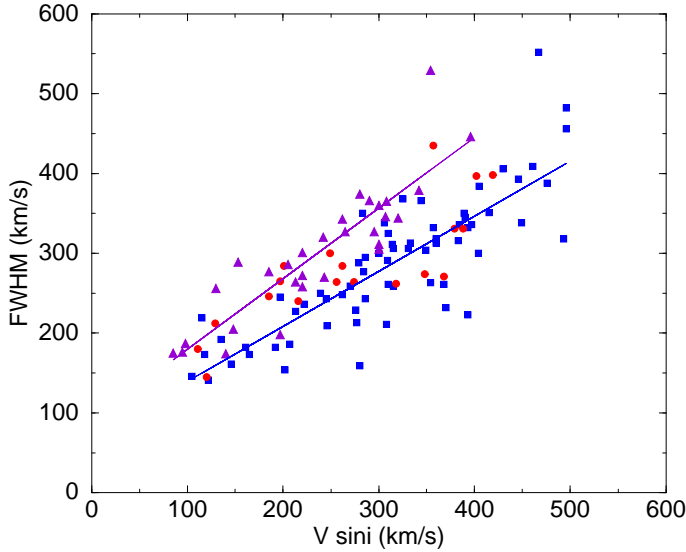


Fig. 3. FWHM of the $H\alpha$ emission line as a function of $V \sin i$ for Be stars with symmetric $H\alpha$ profiles and $EW\alpha > 20 \text{ \AA}$. Squares correspond to Be stars in the SMC, circles to Be stars in the LMC from Paper I, and triangles to Be stars in the MW from Dachs et al. (1992), Andrillat & Fehrenbach (1982) and Andrillat (1983). The linear regression for samples in the SMC and MW is shown.

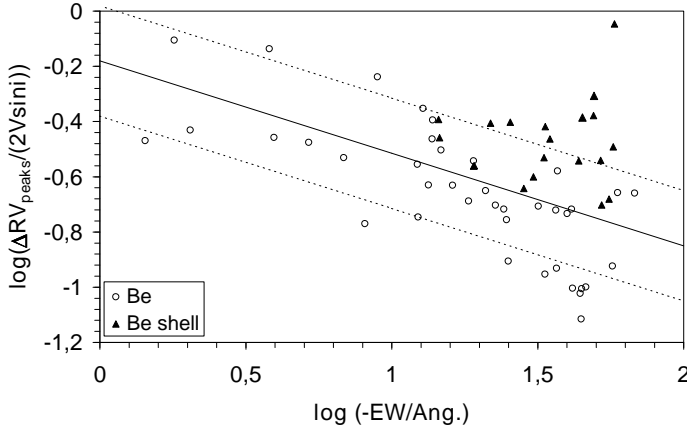


Fig. 4. Peak separation velocity of the $H\alpha$ CS emission line as a function of its equivalent width. Filled triangles correspond to Be-shell stars and open circles to Be stars. The solid line represents the mean correlation from Zamanov et al. (2001), with dashed lines showing the dispersion.

Table 2. Percentage of Be stars. Top: in open clusters. Bottom: in the field. In field A, we exclude NGC330 and the area covered by the study of Keller et al. (1999), and in field B, we exclude only the clusters instead of the entire area studied by Keller et al. (1999).

Cluster	$\log(t)$	Nstars	NBe	$N(\text{Be})/N(\text{B}+\text{Be})\%$
NGC306	7.9 ± 0.2	8	3	38 ± 12
OGLE-SMC99	7.8 ± 0.2	10	4	40 ± 10
Range				20-40
Area		Nstars	NBe	$N(\text{Be})/N(\text{B}+\text{Be})\%$
Field A		178	51	~ 22
Field B		180	78	~ 30
Average field				26 ± 4

3.2.3. Proportion of Be stars

As in the LMC (Martayan et al. 2006c), we determine the percentage of Be stars in the SMC found on the one hand in the observed clusters and OB concentrations and on the other hand in the field close to NGC330. “Be stars” are all non-supergiant O, B and early A-type stars that have shown some emission in their Balmer lines at least once (Jaschek & Egret 1982). This definition is also used here. We have removed from the statistics all the Be stars intentionally observed from Keller et al. (1999), or Grebel et al. (1992) or preselected from our ESO-WFI survey (Martayan et al. 2006a), to remove any bias.

The ratios of Be stars in the clusters and in the field surrounding NGC330, but excluding NGC330 itself, are given in Table 2.

Due to the characteristics of the instrumentation, which do not allow to position many fibres in a small angular size region (typically $\leq 1'$), and due to the characteristics of our survey and the variable nature of the Be phenomenon, the above results should be considered as a rough estimate of the frequency of Be stars.

With FLAMES observations, the use of field stars is suited because the number of observed stars is higher and ages can be averaged out. The proportion of Be stars, which is $26 \pm 4\%$ in fields in the SMC, has to be compared to the one obtained for the LMC with the same methods : $17.5 \pm 2.5\%$ (Paper I).

4. Variability

4.1. Binaries

We search for spectroscopic binaries (SB) among our sample. As the observations have been carried on the same day or within a 1-day interval and as only two spectra (one blue and one red) for each star are generally available, it is not possible to perform a similar search as in the LMC (Paper I). However, 8 spectroscopic binaries with 2 spectra (SB2) have been identified. Moreover, we searched for photometric binaries in the light curves of the 280 stars of the GIRAFFE survey identified in the MACHO and OGLE databases from their coordinates within a radius smaller than $1''$. Among the 13 photometric binaries found, 8 were not known as binaries before and 4 of them are SB2, 2 have a Be component. All the systems are compounds with 1 or 2 B-type stars, excepted SMC5.002807, which has a cold supergiant component (see Sect. A.3 for this latter object).

The orbital period of the systems is determined using 3 different methods: the CLEAN algorithm (Roberts et al. 1987), the Least Squares method and the PDM method (Stellingwerf 1978) with an accuracy of 10^{-6} d. Results are given in Table 3. Illustrations of the most characteristic systems, associated with their MACHO light curve when available, are shown in Figs 5 to 12. The light curve magnitudes are expressed in instrumental units.

In Table 4, we present additional parameters on the binaries. In this table, the ephemeris have been calculated with the primary eclipse at phase 0. The phases at which the blue and red spectra were obtained are also indicated. In the case of rather equal minima it has been difficult to pinpoint the one corresponding to the primary eclipse.

Table 3. Binaries stars in the SMC. The orbital period is given in days. The accuracy on the radial velocities of blue He I lines is $\pm 10 \text{ km s}^{-1}$. The last column provides some additional information: “cl8” is for the star projected onto the open cluster OGLE-SMC99. EB means Eclipsing Binary, SB2 is for spectroscopic binary with two spectra, “ell” means ellipsoidal binary. Note that the star SMC5_016461 was observed twice within 11 months.

Star	MACHO	α (2000)	δ (2000)	Vmag	P(d)	RV1 (km s^{-1})	RV2 (km s^{-1})	Comments
SMC5_000977	207.16205.63	00 54 06.550	-72 14 47.31	16.7	3.128	+8	+ 253	SB2, EB
SMC5_002807	207.16373.18	00 56 09.420	-72 28 09.30	14.6	454.959	+160		cool Sg, EB ¹
SMC5_003789	207.16203.202	00 53 26.690	-72 22 07.40	17.6	2.087	+42		Be, EB
SMC5_004477	207.16375.7	00 56 11.620	-72 18 23.70	14.7	4.480	-42		EB, SB2, eccentric ²
SMC5_004534	207.16318.41	00 55 40.340	-72 17 50.90	16.4	4.051	+167		EB
SMC5_013723	207.16259.277	00 54 53.330	-72 28 12.20	17.5	2.059	+134		cl8, EB ¹
SMC5_016461	207.16316.21	00 55 49.619	-72 25 27.43	14.9	54.317	+95		Be, ell?, EB, SB1-2?
						+83		
SMC5_020391	207.16374.9	00 56 23.580	-72 21 23.60	15.0	2.320	+85	+216	SB2, EB ²
SMC5_023571	207.16375.29	00 56 51.090	-72 17 37.70	15.9	3.534	+63	+288	ell, EB, SB2
SMC5_023641	207.16375.38	00 56 34.250	-72 17 37.30	15.9	2.010	-67	+293	SB2, EB
SMC5_049816	207.16374.65	00 56 19.270	-72 21 03.50	16.6	0.664	-59	+380	SB2, EB ³
SMC5_052516	207.16376.67	00 56 50.579	-72 16 50.85	16.7		+17	+253	SB2
SMC5_052663	207.16319.70	00 55 57.859	-72 16 36.95	17.1		+53	+278	SB2
SMC5_074928	207.16318.129	00 55 09.195	-72 17 13.65	17.3	2.137	+200		ell, EB
SMC5_084353	207.16204.47	00 53 54.750	-72 18 29.50	16.2	1.557	+128		EB

1: Also observed by Wyrzykowski et al. (2004) with OGLE, P(SMC5_002807)=452.295d, P(SMC5_013723)=2.059d.

2: Also observed by Bayne et al. (2002), catalogue MOA, P(SMC5_004477)=4.482d, P(SMC5_020391)=2.320d.

3: Also observed by Samus & Durlevich (2004), star found as a W UMa with P=0.6d.

Table 4. Binaries stars in the SMC. For each eclipsing binary, the ephemeris is listed in col. 2 (phase 0 at the primary eclipse), the phases corresponding to the spectra are given in cols. 3 and 4, the phase of the secondary eclipse in col. 5, the intensity ratio of the 2 minima in col. 6 and the number of the corresponding figure in col. 7.

Star	Ephemeris	phase1	phase2	phase 2nd eclipse	Imini2/Imini1	Figure
SMC5_000977	MJD48857.0852 + 3.127654E	0.87	0.19	0.48	0.85	5
SMC5_003789	MJD48855.3943 + 2.087258E	0.13	0.65	0.49	~0.46	6
SMC5_004477	MJD48856.3937 + 4.479996E	0.19	0.20	0.33	0.66	6
SMC5_004534	MJD48858.1849 + 4.051494E	0.01	0.03	0.50	0.38	7
SMC5_013723	MJD48856.0050 + 2.059270E	0.40	0.92	0.48	0.55	7
SMC5_016461	MJD48865.8675 + 54.337490E	0.87	0.87	0.48	~0.86	8
		0.82	0.84			
SMC5_020391	MJD49145.5595 + 2.320051E	0.92	0.96	0.50	0.95	9
SMC5_023571	MJD48857.8867 + 3.534556E	0.22	0.25	0.52	0.56	9
SMC5_023641	MJD48855.0948 + 2.009626E	0.69	0.74	0.50	0.85	10
SMC5_049816	MJD49144.3831 + 0.663033E	0.85	0.46	0.50	0.98	12
SMC5_074928	MJD49144.1543 + 2.137252E	0.50	0.96	0.50	0.82	12
SMC5_084353	MJD49144.4066 + 1.557259E	0.52	0.57	0.50	0.57	12

4.2. Short-term variability in Be stars

In a preliminary analysis of the MACHO light curves Martayan et al. (2007a) discovered 13 short-period variables among Be stars in the SMC. We reanalysed the same time series in an attempt to refine these periods and to detect additional ones. The tools used for this analysis are Period04 (Lenz & Breger 2005), the CLEAN algorithm (Roberts et al. 1987) and the Least Squares method. In order to know if the detected frequencies are significant or not, we follow the signal to noise ratio (SNR) criterion described in Breger et al. (1993). All the detected frequencies presented in this study fulfill the SNR requirement, i.e. have a SNR greater than 4.

The time span of the observations is ~ 2690 d in the majority of the stars, and thus, the resolution in frequency is $\sim 0.00037 \text{ c d}^{-1}$. The determination of the error in frequency has been obtained with Period04, which follows the equations derived by Montgomery & O’Donoghue (1999). In our case, the estimate of the error in frequency, accounting for the correlation in the residuals (Schwarzenberg-Czerny 1991), is of the order of $1 - 5 \times 10^{-5} \text{ c d}^{-1}$.

We found 9 multi-periodic and 4 mono-periodic stars. The results of the spectral analysis are reported in Table 5. Amplitudes are given in this table only for the b filter, although the same analysis was applied to the dataset for the r filter. Only frequencies detected in both filters were considered as certain. Phase diagrams of the 13 Be stars folded with the detected frequencies are displayed in Figs. 13 to 20. Additional comments on those Be stars are given in Appendix C.

5. Discussion

5.1. Proportion of Be stars versus metallicity

The comparison of the proportions of Be stars in the SMC and LMC to the MW is a difficult issue.

In clusters and OB associations of the Magellanic Clouds, it is not easy to give any firm conclusions from our study about the dependence of the rates of Be stars on the metallicity because the number of stars observed in each cluster is low (≤ 15) and the dispersion in the rates of Be stars is high. The only estimates for clusters in these galaxies have been derived from photometry.

Table 5. Short-term photometric variability of Be stars in the SMC. The EIS names and MACHO numbers of the studied stars are given in cols. 1 and 2, the spectral types taken from Martayan et al. (2007a) in col. 3, the detected frequencies (in c d^{-1}) in cols. 4 and 5, the amplitudes (in mmag) of the corresponding frequencies for the b filter in col. 5 and 6 and additional information in col. 7. Comments: ‘**’ indicates that the star was pre-selected from ESO/ WFI survey (Martayan et al. 2006a). ‘limit’ indicates that the difference between the two detected frequencies is similar to the resolution in frequency and thus, the second frequency is at the limit of detectability. f_{Balona} stands for frequencies (in c d^{-1}) previously obtained by Balona (1992).

Star	MACHO	Sp. T.	f1	f2	Amp. f1, f2	Comments
SMC5_002232	207.16372.22	B2III	1.32661	1.32616	24, 15	** , limit
SMC5_003296	207.16373.5496	B2IV	2.00320		8	
SMC5_013978	207.16373.58	B3III	1.37946	0.59335	16, 14	$f_{\text{Balona,N964}}=1.361$
SMC5_014212	207.16259.29	B2III	1.27691		24	**
SMC5_014727	207.16373.63	B2IV	1.12991		17	$f_{\text{Balona,N585}}=1.120$
SMC5_016523	207.16316.30	B2III	1.29297	1.29344	40, 24	limit
SMC5_016544	207.16373.129	B2IV	1.70774	1.64993	30, 25	
SMC5_021152	207.16147.14	B2III	0.98514	1.00443	19, 19	
SMC5_037013	207.16315.26	B2III	1.18153	1.21709	15, 9	**
SMC5_037162	207.16259.57	B2III	0.88531	0.90612	37, 19	OGLE005440.73-722752.4 ($f=0.443 \text{ cd}^{-1}$)
SMC5_043413	207.16315.41	B2IV	2.00716		7	
SMC5_082042	207.16375.41	B3III	2.48834	1.16625	19, 17	
SMC5_082941	207.16203.47	B3III	0.62483	0.62525	51, 12	$f_3=0.15324$ not a pulsation

Wisniewski & Bjorkman (2006) find an increase of the proportion of Be stars to B stars with decreasing metallicity in open clusters.

On the contrary in the field of the Magellanic Clouds for which our samples are highly significant our results on proportion of Be stars are robust. For field stars in the MW Zorec & Briot (1997) obtained a 20% value considering several decades of Galactic searches for Be stars, and several corrections for different sources of incompleteness of the currently known Be star samples. Conversely, the proportions we have obtained for the SMC and LMC are made from a single epoch survey, in which many Be stars are likely to be missed due to the non-permanent nature of the Be phenomenon. Therefore, both kind of values are not directly comparable. It is difficult to estimate what would be the result of a single epoch survey for Be stars in the Galaxy, but it will certainly be lower than 20%, probably between 10 and 15%.

If we consider that the probable value in the MW for a single epoch survey is lower than 15%, our estimates in the field of the MC (17.5% in the LMC and 26% in the SMC) indicate an increase of the proportion of Be stars with decreasing metallicity. Note that Keller et al. (1999) did not find such an increase but the fields observed by these authors were smaller and closer to the clusters than ours while Evans et al. (2006), from a restricted sample also obtained with the FLAMES-GIRAFFE instrumentation, found a proportion of Be stars similar to ours in the LMC and in the SMC.

The higher proportion of Be stars in the SMC could be explained by the higher ratio of angular velocity to breakup velocity Ω/Ω_c found in this galaxy ($\Omega/\Omega_c=95\%$, Paper II) compared to the ones in the LMC and MW ($\Omega/\Omega_c=85\%$ and 80% respectively, Paper II). Our observational results support predictions by Maeder & Meynet (2000), which link the occurrence of Be stars to enhanced stellar rotation for B-type stars in low metallicity environments.

5.2. Be stars as pulsators

Several authors have previously investigated the pulsational behavior of Be stars in the SMC, by means of photometric

and spectroscopic techniques, with negative results. Balona (1992) conducted a photometric variability study of Be stars in the region of the young open cluster NGC330 in the SMC. He found many of them to be short-period variables, but he was able to find only one period in each star. He concluded that the short-term variability is produced by rotational modulation of the light curve caused by inhomogeneities in the stellar photosphere. Baade et al. (2002) obtained time-resolved high-resolution spectroscopy of two bright Be stars close to NGC330. They failed to find line-profile variability, and their analysis cast doubts on the presence of pulsations in these two stars.

Our finding of photometric multi-periodicity in 9 SMC Be stars clearly shows that (1) they are variable, and (2) they are pulsating stars. In particular, the detected periods fall in the range of SPB-type pulsating modes (from 0.40 to 1.60 days).

The current theoretical models do not predict the presence of pulsational instabilities in massive stars at metallicities much lower than the Galactic one (Pamyatnykh 1999). However, these models have recently been challenged by several observational results. Kołaczowski et al. (2004) detected some β Cephei and SPB stars in the LMC. Recently, Fabrycky (2005) and Schmidtke et al. (2004) have also detected multiple periods in high mass X-ray binaries with a Be primary component (Be/X system) in the SMC. These results point towards the necessity of new modeling or improved determination of the opacities used in current theoretical models.

In an attempt to investigate the discrepancies between theory and observations, Miglio et al. (2006) have analyzed the effect of uncertainties in the opacity computations on the excitation of pulsation modes in B-type stars. Computations for a low metallicity ($Z=0.005$) showed that none of the different opacities with different mixtures predicts β Cep-type pulsations, whereas they found excited SPB-type modes when considering the recently updated OP opacity with the new metal mixture with Fe enhancement. The instability strip is compatible with the position of the studied stars in our work (M.A. Dupret, priv. comm.). However, the metallicity of NGC330 and its surrounding field is $Z=0.002$ (see Maeder et al. 1999, and references

therein), which is lower than the lowest metallicity used by Miglio et al. (2006).

6. Conclusions

Medium-resolution spectroscopic observations of a large sample of B and Be stars in the SMC-NGC330 region are presented. 131 Be stars were identified in the field as well as in small clusters and OB associations.

Characteristics of the $H\alpha$ emission line were investigated through spectral parameters (FWHM α , EW α , peak separation). The CS envelope of Be stars seems to be rotationally supported. Higher EW α and lower FWHM α values are found for a large fraction of Be stars in the SMC compared to the LMC and MW. It could indicate the presence of more extended CS envelopes around a fraction of Be stars in the SMC.

The proportion of field Be stars compared to B-type stars is found to be slightly higher in the SMC (26%) than in the LMC (17.5%) and MW (estimated <15% for a single epoch survey). This result could be explained by the ratios of angular velocities Ω/Ω_c of Be stars, which are close to the critical value in the SMC (see Paper II). Thus, the decrease in metallicity over Ω/Ω_c seems to influence the occurrence of the Be phenomenon.

We have also found 13 photometric binaries by cross-correlation with the MACHO and OGLE databases. Among them, 8 are newly discovered, 2 include a Be star, 4 are SB2. For each of these stars, the period of the system is given. In addition, we discovered 2 SB2 in the GIRAFFE spectra, without any photometric variations in the MACHO database. Finally, we studied the short-term variability of Be stars in the SMC and we found a periodicity for 13 of the observed Be stars. Moreover, for the first time, we found evidence for multi-periodicity (2 frequencies) for 9 of them. Such multi-periodicity, which is the signature of stellar pulsations, had never been found so far in Be stars in such a low metallicity environment. Our result points toward the necessity of modeling of pulsation instabilities in B-type stars at the metallicity of the SMC.

Acknowledgements. We would like to thank Dr D. Baade for very fruitful discussions. This research has made use of the Simbad database and VizieR database maintained at CDS, Strasbourg, France. This paper utilizes public domain data originally obtained by MACHO Project, whose work was performed under the joint auspices of the U.S. Department of Energy, National Security Administration by the University of California, Lawrence Livermore National Laboratory under contract No. W-7405-Eng-48, the National Science Foundation through the Center for Particle Astrophysics of the University of California under cooperative agreement AST-8809616, the Mount Stromlo and Siding Spring Observatory, part of the Australian National University.

References

Andrillat, Y. 1983, A&AS, 53, 319
 Andrillat, Y. & Fehrenbach, C. 1982, A&AS, 48, 93
 Arp, B. H. 1959, AJ, 64, 254
 Baade, D., Rivinius, T., Štefl, S., & Kaufer, A. 2002, A&A, 383, L31
 Balona, L. A. 1992, MNRAS, 256, 425
 Bayne, G., Tobin, W., Pritchard, J. D., et al. 2002, MNRAS, 331, 609
 Breger, M., Stich, J., Garrido, R., et al. 1993, A&A, 271, 482
 Dachs, J., Hanuschik, R., Kaiser, D., Ballereau, D., & Bouchet, P. 1986, A&AS, 63, 87
 Dachs, J., Hummel, W., & Hanuschik, R. W. 1992, A&AS, 95, 437
 Evans, C. J., Lennon, D. J., Smartt, S. J., & Trundle, C. 2006, A&A, 456, 623

Fabrycky, D. 2005, MNRAS, 359, 117
 Grebel, E. K. & Richtler, T. 1992, A&A, 253, 359
 Grebel, E. K., Richtler, T., & de Boer, K. S. 1992, A&A, 254, L5
 Grundstrom, E. D. & Gies, D. R. 2006, ApJ, 651, L53
 Hanuschik, R. W., Kozok, J. R., & Kaiser, D. 1988, A&A, 189, 147
 Hummel, W., Gässler, W., Muschelklok, B., et al. 2001, A&A, 371, 932
 Hummel, W., Szeifert, T., Gässler, W., et al. 1999, A&A, 352, L31
 Jaschek, M. & Egret, D. 1982, in IAU Symp. 98: Be Stars, ed. M. Jaschek & H.-G. Groth, 261
 Keller, S. C. 1999, AJ, 118, 889
 Keller, S. C., Wood, P. R., & Bessell, M. S. 1999, A&AS, 134, 489
 Kołaczowski, Z., Pigulski, A., Soszyński, I., et al. 2004, in ASP Conf. Ser. 310: IAU Colloq. 193: Variable Stars in the Local Group, ed. D. W. Kurtz & K. R. Pollard, 225
 Kučinskas, A., Vansevičius, V., Sauvage, M., & Tanabé, T. 2000, A&A, 353, L21
 Lamers, H. J. G. L. M., Zickgraf, F.-J., de Winter, D., Houziaux, L., & Zorec, J. 1998, A&A, 340, 117
 Leisy, P. & Dennefeld, M. 1996, A&AS, 116, 95
 Leisy, P. & Dennefeld, M. 2006, A&A, 456, 451
 Lenz, P. & Breger, M. 2005, Communications in Asteroseismology, 146, 53
 Lindsay, E. M. 1961, AJ, 66, 169
 Maeder, A., Grebel, E. K., & Mermilliod, J.-C. 1999, A&A, 346, 459
 Maeder, A. & Meynet, G. 2000, A&A, 361, 159
 Maeder, A. & Meynet, G. 2001, A&A, 373, 555
 Martayan, C., Baade, D., Hubert, A.-M., et al. 2006a, SF2A-2006, 481
 Martayan, C., Floquet, M., Hubert, A.-M., & Mekkas, M. 2007a, in Astronomical Society of the Pacific Conference Series, Vol. 361, Active OB-Stars: Laboratories for Stellar and Circumstellar Physics, ed. A. T. Okazaki, S. P. Owocki, & S. Stefl, 460
 Martayan, C., Frémat, Y., Hubert, A.-M., et al. 2006b, A&A, 452, 273
 Martayan, C., Frémat, Y., Hubert, A.-M., et al. 2007b, A&A, 462, 683
 Martayan, C., Hubert, A. M., Floquet, M., et al. 2006c, A&A, 445, 931
 Meilland, A., Stee, P., Vannier, M., et al. 2007, A&A, 464, 59
 Meynet, G. & Maeder, A. 2000, A&A, 361, 101
 Meynet, G. & Maeder, A. 2002, A&A, 390, 561
 Meyssonnier, N. & Azzopardi, M. 1993, A&AS, 102, 451
 Miglio, A., Bourge, P., Montalbán, J., & Dupret, M. 2006, ArXiv Astrophysics e-prints 0611944
 Momany, Y., Vandame, B., Zaggia, S., et al. 2001, A&A, 379, 436
 Montgomery, M. & O'Donoghue, D. 1999, Delta Scuti Newsletter, 13, 28
 Neiner, C., Floquet, M., Hubert, A. M., et al. 2005, A&A, 437, 257
 Nussbaumer, H., Schmid, H. M., & Vogel, M. 1989, A&A, 211, L27
 Pamyatnykh, A. A. 1999, Acta Astronomica, 49, 119
 Pasquini, L., Avila, G., Blecha, A., et al. 2002, The Messenger, 110, 1
 Roberts, D. H., Lehar, J., & Dreher, J. W. 1987, AJ, 93, 968
 Robertson, J. W. 1974, A&AS, 15, 261
 Samus, N. N. & Durlevich, O. V. 2004, VizieR Online Data Catalog, 2250
 Schmid, H. M. 1989, A&A, 211, L31
 Schmidtke, P. C., Cowley, A. P., Levenson, L., & Sweet, K. 2004, AJ, 127, 3388
 Schwarzenberg-Czerny, A. 1991, MNRAS, 253, 198
 Sebo, K. M. & Wood, P. R. 1994, AJ, 108, 932
 Stellingwerf, R. F. 1978, ApJ, 224, 953
 Sterken, C., Vogt, N., & Mennickent, R. 1994, A&A, 291, 473
 Szymanski, M. K. 2005, Acta Astronomica, 55, 43
 Walker, G. A. H., Kuschnig, R., Matthews, J. M., et al. 2005a, ApJ, 635, L77
 Walker, G. A. H., Kuschnig, R., Matthews, J. M., et al. 2005b, ApJ, 623, L145
 Wisniewski, J. P. & Bjorkman, K. S. 2006, ApJ, 652, 458
 Wyrzykowski, L., Udalski, A., Kubiak, M., et al. 2004, Acta Astronomica, 54, 1
 Zamanov, R. K., Reig, P., Martí, J., et al. 2001, A&A, 367, 884
 Zorec, J. & Briot, D. 1997, A&A, 318, 443

Appendix A: Peculiar objects

In this section, we present the 3 peculiar emission-line objects (non Be stars) observed on October 21, 22 and 23, 2003.

A.1. SMC5_037102

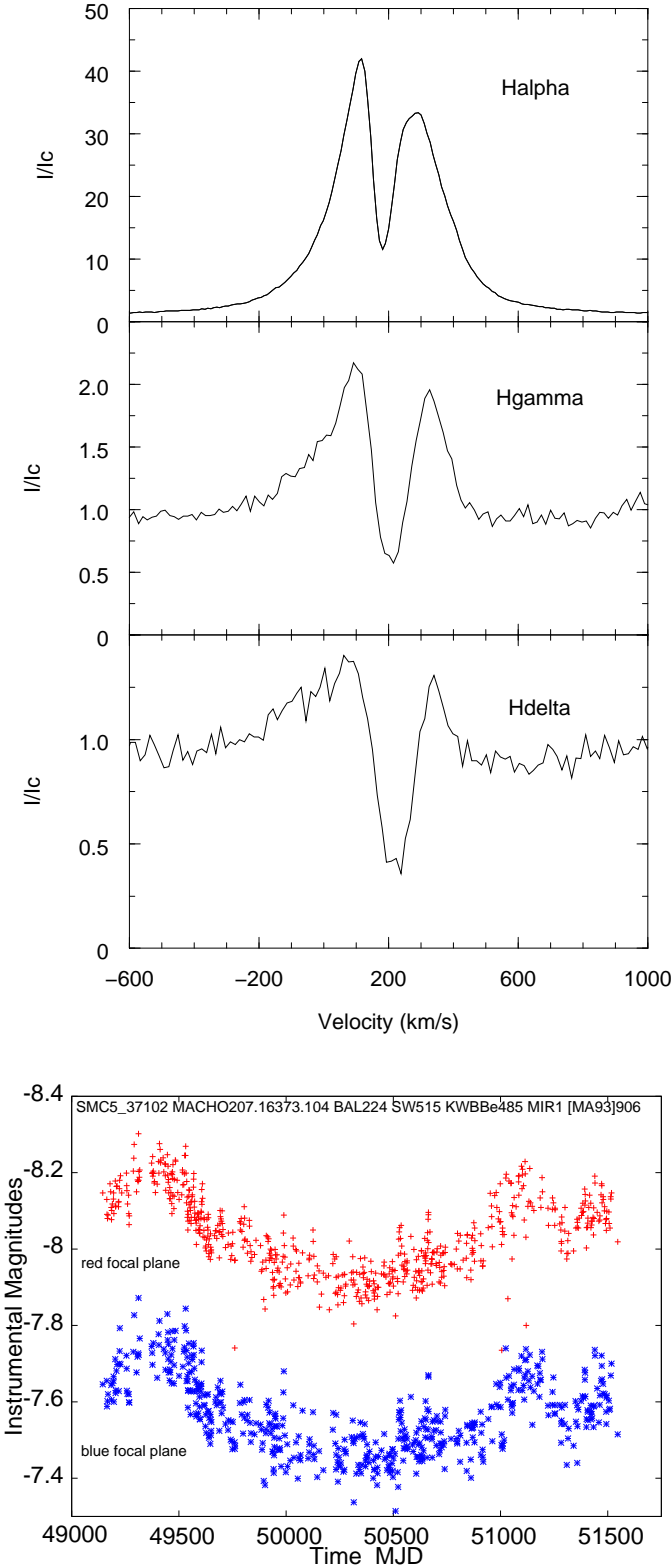


Fig. A.1. SMC5_037102. Top : Balmer emission lines $H\alpha$, $H\gamma$ and $H\delta$. Bottom: MACHO light-curves in the blue and red bands.

The star is also known as KWBB485 (Keller et al. 1999), BAL 224 (Balona 1992), SW 515 (Sebo & Wood 1994), and [MA93] 906

(Meyssonnier & Azzopardi 1993). It has been reported as an IR object (MIR1) in Kučinskas et al. (2000). From VLT-FORS1 low resolution spectroscopic observations Hummel et al. (1999) suggested that the absence of emission in $He I$ lines and the strong Balmer decrement could indicate that this star has a shell of gas cooler than 5000 K. Thanks to ISOCAM observations Kučinskas et al. (2000) found a prominent mid-IR excess consistent with a dust shell of low temperature (360 K). Without discarding the possibility that the object may be an isolated Ae/Be star, they, nevertheless, favoured a supergiant Be or an AGB star to explain visual and mid-IR photometry at once. The star also varied photometrically. According to Balona (1992) it displayed a fading of 0.2 mag in 1991 and a rapid variability close to 1 day but without any period satisfactorily fitting the data. We investigate the star's variability thanks to the MACHO and OGLE databases; 2 strong outbursts, separated by smaller ones without any periodic recurrence, occurred on a time-scale of about 3100 days and with a 0.4 mag amplitude (see Fig. A.1). No short period can fit the data in spite of rapid variability close to a 1-d time-scale.

The GIRAFFE red spectrum is dominated by a very strong asymmetric double-peaked $H\alpha$ emission line ($EW = 360 \text{ \AA}$, $V/R = 1.24$) affected by a shell feature. The R component seems to be larger than the blue one. In the blue spectrum $H\gamma$ and $H\delta$ also display $V/R > 1$, but the blue wing of their emission is highly complex compared to the red one. The mean value of the RV of the shell component of $H\alpha$, $H\gamma$ and $H\delta$ (see Table A.1) is $+193 \text{ km s}^{-1}$; it is red-shifted with respect to the emission (Fig. A.1). Spectral parameters of the H lines are reported in Table A.1 and compared to the ones obtained by Hummel et al. (1999). We confirm the strong Balmer decrement.

Table 6 gives the identification of emission and absorption lines. Thanks to the resolution used in this study, it is possible, for the first time, to identify $Fe II$ and $[Fe II]$ emission lines as well as the $[S II]$ nebular lines 4068, 6717 and 6731; however, the nebular $[N II]$ lines 6548 and 6583 are not detected in the spectrum. The mean radial velocity (RV) of emission lines is $+165 \pm 10 \text{ km s}^{-1}$ indicating that this object belongs to the SMC. The FWHM of metallic emission lines is about 80 km s^{-1} . We do not notice any significant difference between RVs and FWHMs of permitted and forbidden emission lines. In spite of the low S/N ratio ($S/N \simeq 20$ in the continuum) and the presence of numerous metallic emission lines it has been possible to measure RVs of absorption lines identified as $He I$ lines 4026, 4388, 4471 and 6678 and $O II$ (see Table 6), however $Mg II$ 4481 line is absent. All these identifications indicate that the central object is a hot star. All the helium lines are strongly red-shifted except $He I$ 4388. By comparison with corresponding profiles of B stars having a similar radial velocity we can conclude that this red-shift is in fact due to $He I$ emission which fills in the blue part of the $He I$ photospheric lines. $He I$ line profiles as well as Balmer emission line profiles may thus be explained by an accretion disk (Hummel et al. 1999).

In conclusion this star shows common characteristics with the pre-main sequence B[e] stars following Lamers et al. (1998): presence of $Fe II$ and $[Fe II]$ emission lines with FWHM lower than 100 km s^{-1} , spectroscopic evidence of accretion or in-fall, large irregular photometric variations on time scale from 1 to 1000 days.

Table A.1. Spectral parameters of Balmer lines in SMC5_037102. Values between brackets are taken from Hummel et al. (1999).

	$H\alpha$	$H\gamma$	$H\delta$
$RV_V (\pm 20) \text{ km s}^{-1}$	104 [140 ± 50]	86	62
$RV_{shell} (\pm 20) \text{ km s}^{-1}$	173	201	207
$RV_R (\pm 20) \text{ km s}^{-1}$	276 [301 ± 50]	317	327
$FWHM (\pm 20) \text{ km s}^{-1}$	320 [443 ± 50]	410	600
I_V	41.8 [18.6]	2.2	1.4
I_R	33.4 [15.2]	1.9	1.3
Mean I	37.6 [16.9]	2.1	1.4
$EW (\pm 20) \text{ \AA}$	360 [202 ± 20]		

A.2. SMC5_081994

This star, also known as KWBB4154, is the planetary nebula SMC SMP 21 in Lindsay (1961). From its spectral characteristics it has been classified as a type I PNe by Leisy & Dennefeld (1996, 2006).

These authors claimed that the central star could belong to a binary system. We present the first spectroscopic observations of this object obtained at medium resolution. The identification of emission lines and their corresponding flux are given in Table 7. The flux have been obtained by fitting a gaussian function. The blue and red spectrum are displayed in Fig. A.2. The mean FWHM of nebular and emission lines is 1.18 Å.

Thanks to the good quality of the spectra it is possible to distinguish a triple structure at the foot of the most intense emission lines $H\alpha$, $H\gamma$, $H\delta$ and nebular lines of [NII], [SII] and [OIII] (see Fig. A.3). Each central emission peak is flanked by 2 weak emission peaks, which are about symmetric around the central one ($\pm 150 \text{ km s}^{-1}$ in the red domain and $\pm 120 \text{ km s}^{-1}$ in the blue domain). These secondary emission peaks could be the signature of matter previously ejected from the central star. In the case of Balmer lines the blue component is about 5.4 times stronger than the red one whereas in the case of nebular lines the two components seem to be of equal intensity.

It has to be noted that we observed broad emission patterns at 6834.74 and 7092.52 Å, which can be identified as Raman scattering by neutral hydrogen of the OVI resonance doublet at 1032 and 1038 Å (Nussbaumer et al. 1989; Schmid 1989).

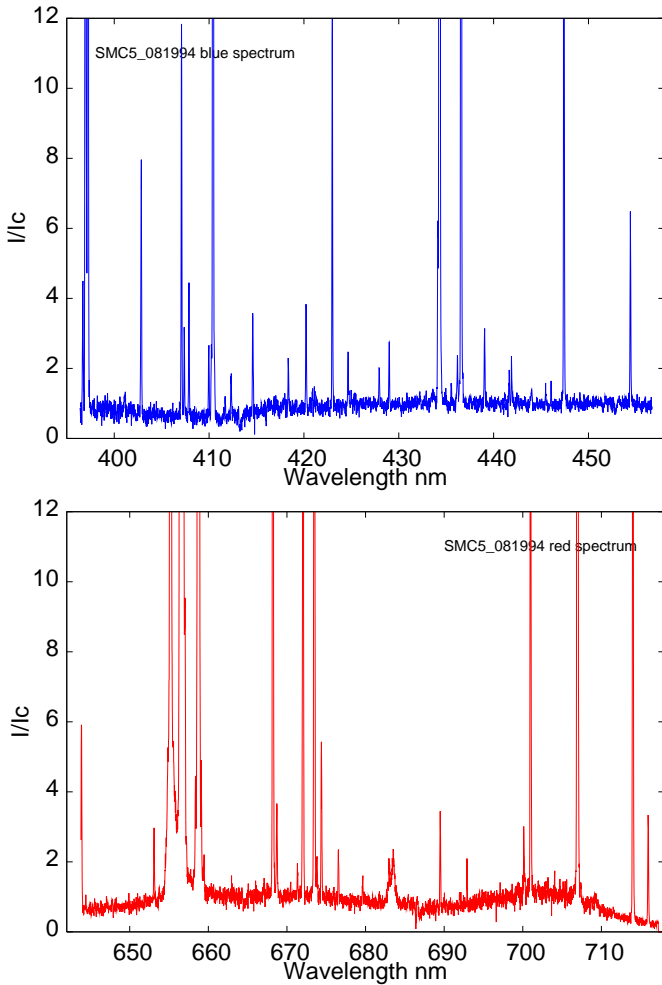


Fig. A.2. Spectrum of the PN SMC5_081994. Top: blue domain. Bottom: red domain.

A.3. SMC5_2807

This star is also known as KWBB44 (Keller et al. 1999), ROBB31 (Robertson 1974), BAL317 (Balona 1992), ARP2 (Arp 1959) and SW77 (Sebo & Wood 1994). These studies are mainly based on photometric surveys and/or low-resolution spectroscopic data. From CCD Strömgren photometry Grebel & Richtler (1992) found that this star

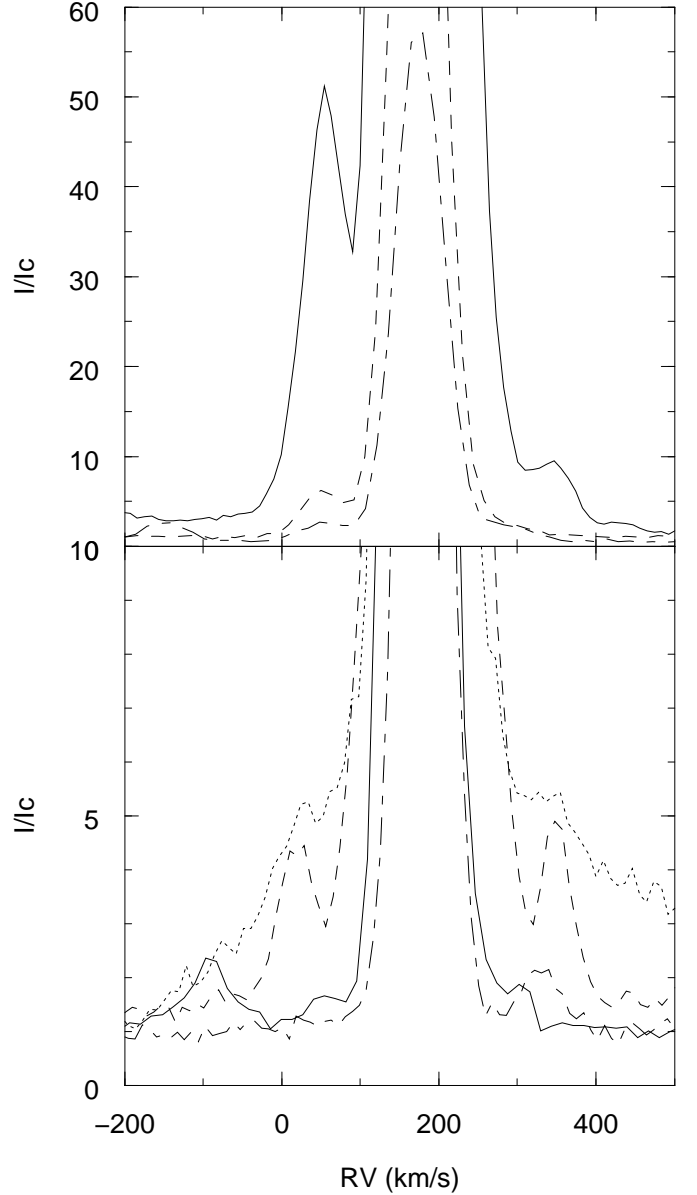


Fig. A.3. Triple structure at the foot of the most intense emission lines in the spectrum of the PN SMC5_081994. Top: Balmer lines. The solid line is $H\alpha$, the dashed line is $H\gamma$ and the dot-dashed line is $H\delta$. Bottom: nebular lines. The solid line is [OIII] 4363, the dotted line is [NII] 6548, the dashed line is [NII] 6583 and the dot-dashed line is [SII] 6730.

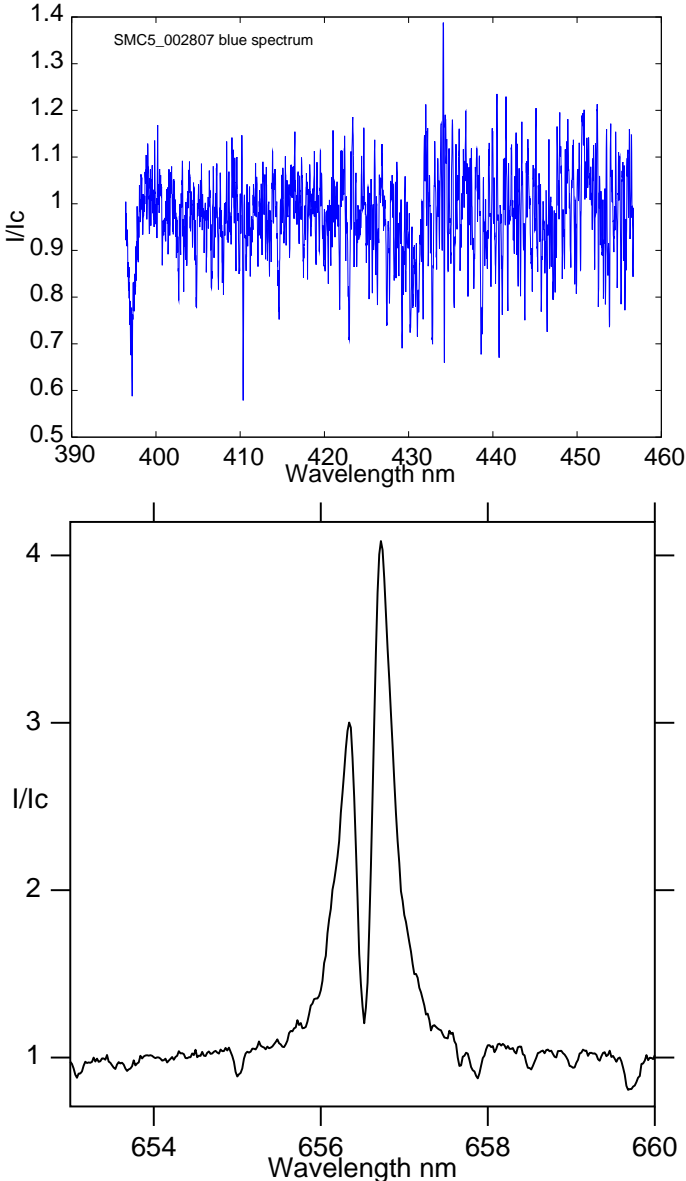
has a very low metallicity: $[M/H] = -2.37$ dex. From a 4-year monitoring in V and I bands with CCD images to search for Cepheids and Long-Period Variables (LPV) Sebo & Wood (1994) detected a 227d-period. Then, from the light curve and a $H\alpha$ spectrum, they investigated the nature of the star and concluded that the star is a foreground binary system consisting of a red supergiant or upper AGB star and a compact star surrounded by a disk where the $H\alpha$ emission line is formed. They estimated the mass $M \simeq 13 M_{\odot}$ and the stellar radius $R \simeq 171 R_{\odot}$ for the red star, the companion would have $M = 1 M_{\odot}$. From broadband IR photometry, Keller (1999) showed that the star is a red supergiant with $T_{\text{eff}} \sim 4355 \text{ K}$ and $\log(L/L_{\odot}) = 3.971$. The star is included in the OGLE catalogue of eclipsing binary stars (Wyrzykowski et al. 2004) which gives a 452.29480-day period. Using MACHO data we find a 454.959-day period (see Sect. 4.1, Table 3), close to the one derived from the OGLE survey.

The GIRAFFE observations in LR02 and LR06 have been obtained at

Table A.2. Characteristics of the $H\alpha$ emission line of SMC5_2807 in the spectra from this study and Hummel et al. (2001).

Date	EW Å	I(V)/Ic	I(R)/Ic	RV(V) km s ⁻¹	RV(R) km s ⁻¹	FWHM km s ⁻¹	Source
2003/10/22	20.7	4.1	3.0	+8	+188	374	this study
1999/11/12	8	1.6	2.1	-70	+240	460	Hummel et al. (2001)

phase 0.07 i.e. out of eclipses (Fig. A.4). We observe a cool star spectrum with $RV_* = +160$ km s⁻¹. Thus this star seems to be a SMC member. The $H\alpha$ emission line shows an asymmetric double profile, with $V < R$ and a deep central absorption, similar to the one shown in Sebo & Wood (1994) and Hummel et al. (2001). However, the spectral parameters of the $H\alpha$ emission line are variable (see Table A.2) and changed between our study and Hummel et al. (2001) who then observed this system in a stage of lower emission. The RV of the narrow deep absorption is +98 km s⁻¹ for $H\alpha$ and +120 km s⁻¹ for $H\gamma$ and $H\delta$ in GIRAFFE spectra. Those features, as well as the double emission in $H\alpha$, are probably formed in a disk which surrounds the secondary star or in a circumbinary disk.

**Fig. A.4.** Spectra of the cool supergiant SMC5_002807, top: blue spectrum; bottom: zoom on $H\alpha$.

Appendix B: Additional comments on binaries

SMC5_016461: This object is a Be-shell star with a strong double $H\alpha$ emission line ($EW_\alpha = 52\text{\AA}$, $Imax \leq 9.5$ with $V < R$). This star was observed twice within an interval of 11 months (2003 and 2004). The blue spectrum displays numerous metallic shell lines of Fe II, Ti II, Cr II and Si II; the stronger Fe II lines are flanked by V and R emission components. In 2004 we observed 2 absorption components in Fe II and Ti II lines ($RV = +81$ and $+115$ km s⁻¹) but only one in He I, Cr II, Mg II and Si II (on average $RV = +83$ km s⁻¹). In the 2003 spectra, the lines are deeper and simple and their average RV is +108 km s⁻¹. The radial velocity of the shell components of the Balmer lines is +126 km s⁻¹ in 2003 and +130 km s⁻¹ in 2004. The accuracy on the RV measurements is ± 2 km s⁻¹.

The MACHO and OGLE data show a periodic variability with $P = 27.1687$ d with a peak to peak amplitude ~ 0.2 mag, but we cannot exclude that the true period could be twice the detected period i.e. $P = 54.3374$ d (see Fig. 8). In this latter case the two minima are not very different from each other. In this picture, this object would belong to the group of β Lyrae type eclipsing variables with long period in which the light curve does not show any plateau and varies continuously. This star has a behavior similar to the one of HD50123 (Sterken et al. 1994): similar light curve, long period, a Be star as primary, relative intensity of the 2 minima. As HD50123, this object could thus be an interacting binary with a Be star as primary, and the companion displaying ellipsoidal variations with a period of 54.3374d. More spectroscopic observations are needed to validate our proposition.

SMC5_052516: The MACHO data do not show any evidence of periodicity. However, the star could be a SB2. The He I lines display either a splitting or an asymmetry (red-winged profile).

SMC5_052663: The MACHO data do not show any evidence of periodicity. However, the star is clearly a SB2 system with a separation in RV of 225 km s⁻¹ (see Fig. 11).

Appendix C: Comments on the individual Be stars

SMC5_013978: Balona (1992) has previously observed this star (number 964 in his list) and found it variable with a frequency of 1.361 c d⁻¹. The large time baseline of the MACHO light curves (~ 2700 d) allows us to refine his frequency and, furthermore, to find an additional frequency (Fig. 14).

SMC5_014727: Balona (1992) has previously observed this star (number 585 in his list) and found it variable with a frequency at 1.120 c d⁻¹. Thanks to the larger time span of the MACHO observations, we are able to refine this frequency (Fig. 15).

SMC5_016544: To confirm the two frequencies found, we folded the light curve with the frequency produced by the beating of the two frequencies, i.e. $f_{\text{beating}} = 1.70774 - 1.64993 = 0.05781$ c d⁻¹ (Fig. 16). This plot shows evidence of beating phenomenon.

SMC5_037013: After prewhitening for the two first frequencies (Fig. 18), we find a significant frequency at $f_3 = 1.18113$ c d⁻¹ (SNR ~ 6). As the difference between f_1 and f_3 is very close to our resolution in frequency and the phase diagram folded with f_3 is very scattered, we consider it as uncertain.

SMC5_037162: OGLE (Wyrzykowski et al. 2004) found a frequency $f = 0.443$ c d⁻¹. From our analysis, we obtained the frequency f_1 , which is twice the OGLE's frequency, and an additional frequency.

SMC5_082941: Note that the frequency f_3 , due to its time-scale (period of 6.526 d), is probably not due to pulsation, but to surface activity or a possible binarity. We also detected an additional frequency at 0.62525 c d⁻¹ which fulfills the SNR requirement.

Online Material

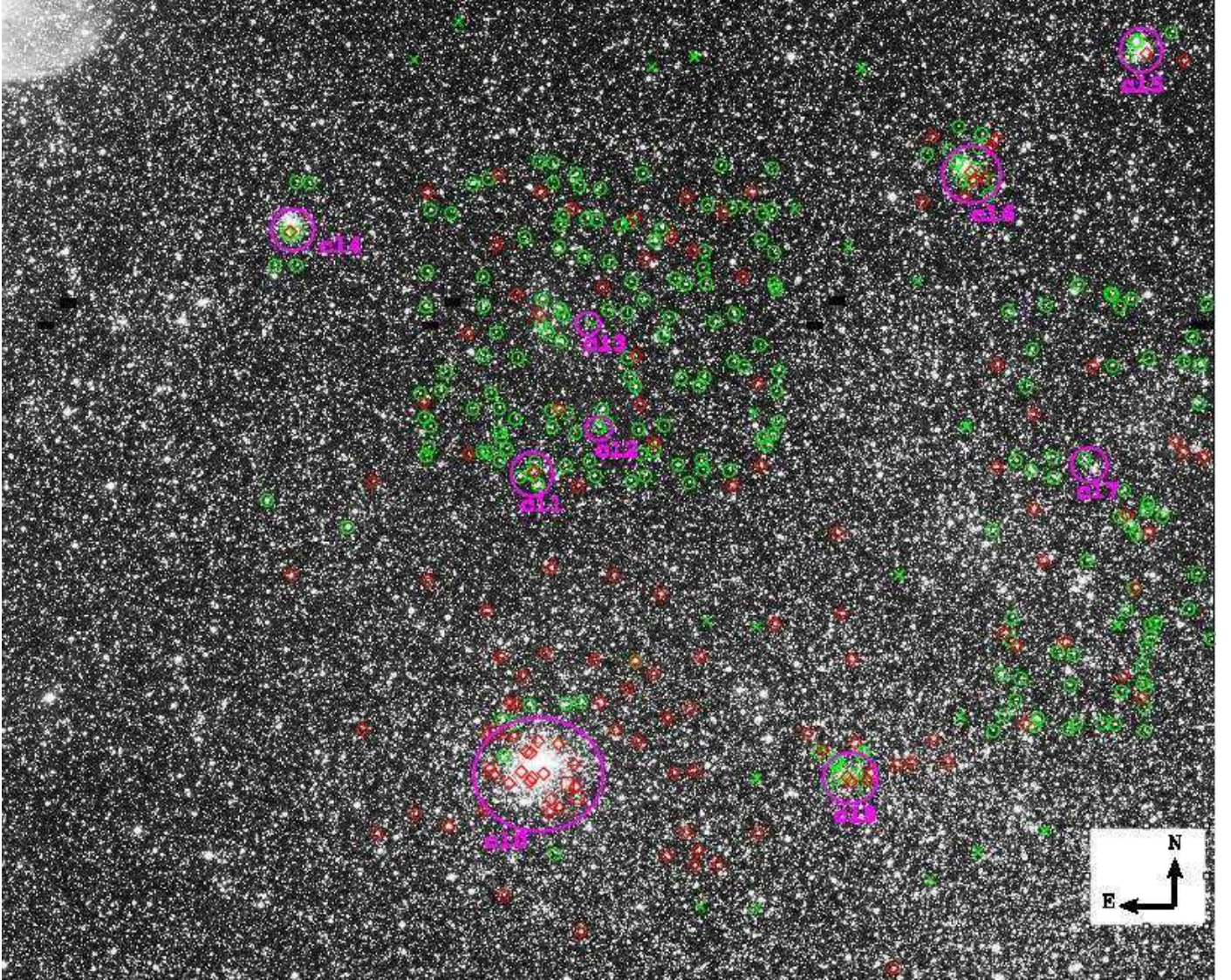


Fig. 1. Part of the SMC5 field from EIS pre-FLAMES survey (Momany et al. 2001). Red diamonds are for Be stars, red squares for the other emission line stars, small green circles are for non-emission line stars (mainly B-type stars), green crosses for the sky fibre positions. The large pink circles indicate the clusters and associations: cl0 for NGC330, cl1 for H86 170, cl2 for [BS95]78, cl3 for SMC ASS39, cl4 for OGLE SMC109, cl5 for NGC299, cl6 for NGC306, cl7 for H86 145, and cl8 for OGLE SMC99.

Table 1. Observational characteristics of Be stars in the SMC. The first column gives the name of the Be star in the EIS catalogue or following our catalogue if the star is not found in the EIS catalogue. In the last column some complementary indications on the spectrum are given: ‘cl’ the star belongs to a cluster, ‘bin’ the star is a binary; ‘sh’ the star shows shell lines; ‘Fe II’ (red or blue lines) and ‘He I’ (red lines) indicate that the corresponding lines present emission components, ‘dble’ and ‘w’ when the corresponding emission is a double peak one and weak respectively; ‘noneb’ no nebular lines have been detected; ‘ α (CS+neb)’ the nebular line is present at H α but cannot be disentangled from the CS emission and ‘ α CS+ α neb’ the H α CS and nebular lines can be disentangled; the mention kXXX is the number of the star in Keller et al. (1999). ‘***’ indicates that the star was pre-selected from the ESO-WFI slit-less study Martayan et al. (2006a). Note that the star SMC5_016461 was observed twice within 11 months interval.

Name	α 2000	δ 2000	Vmag	EW α Å	I(V)	I(R)	Imax	FWHM α km s ⁻¹	Remarks
MHF[S9]47315	00 54 49.559	-72 24 22.35	-	52.73			8.78	232	**, α (CS+neb), He I dble, Fe II
MHF[S9]51066	00 54 50.936	-72 22 34.63	-	52.08			6.76	351	**, α (CS+neb), Fe II dble
SMC5_000476	00 53 23.700	-72 23 43.80	16.36	19.52			5.15	291	α CS+ α neb
SMC5_000643	00 55 44.490	-72 20 38.00	16.30	39.49			8.94:	159	α CS+ α neb
SMC5_002232	00 56 05.560	-72 31 25.68	15.60	57.53			10.89	209	**, α (CS+neb), Fe II
SMC5_002483	00 55 32.170	-72 29 56.70	16.80	39.27			6.73	263	k1064, α CS+ α neb
SMC5_002751	00 56 14.260	-72 28 30.10	15.99	60.54			9.69	259	cl, α (CS+neb), Fe II
SMC5_002825	00 54 41.373	-72 28 02.42	17.43	25.32			5.79	213	cl, α (CS+neb)
SMC5_002957	00 54 45.158	-72 27 13.68	15.28	33.92			6.58	250	**, α (CS+neb), Fe II w
SMC5_002984	00 55 48.780	-72 27 12.70	17.40	14.47	2.67	2.12		438	sh, α CS+ α neb, Fe II
SMC5_003119	00 55 59.900	-72 26 21.30	15.62	39.34			6.93	247	k258, α (CS+neb), Fe II w
SMC5_003296	00 56 15.964	-72 25 15.98	16.83	15.50	3.95	4.03		216	k916, α CS+ α neb
SMC5_003315	00 53 58.250	-72 25 02.60	16.06	19.06	3.12	3.14		393	sh, α CS+ α neb
SMC5_003389	00 55 08.999	-72 24 37.24	16.24	56.98	7.50	7.28		336	**, α CS+ α neb, Fe II dble
SMC5_003537	00 56 50.484	-72 23 40.08	16.27	27.73			5.58	245	**, α CS+ α neb, Fe II?
SMC5_003789	00 53 26.690	-72 22 07.40	17.62	36.45	3.95	3.82?		490	bin, α CS+ α neb
SMC5_003919	00 57 06.510	-72 21 29.55	16.95	46.02			7.00:	311	**, α CS+ α neb
SMC5_004026	00 56 38.660	-72 20 52.80	17.53	28.31	3.81	3.69		452	sh, noneb, Fe II dble
SMC5_004201	00 56 12.270	-72 19 52.90	16.33	69.04			6.13	454	α CS+ α neb, Fe II dble+w
SMC5_004509	00 56 38.767	-72 18 12.67	16.52	12.12			4.07	159	α (CS+neb)
SMC5_004685	00 55 59.850	-72 17 11.40	16.36	25.41			4.91	243	α (CS+neb), Fe II?
SMC5_004982	00 55 24.880	-72 15 30.60	16.29	36.38	6.48:	6.41		259	α CS+ α neb
SMC5_005045	00 54 15.010	-72 15 08.80	15.80	6.84	1.99	1.93		327	α CS+ α neb
SMC5_008231	00 56 04.638	-72 33 41.61	16.26	51.15			6.43	368	**, α (CS+neb), Fe II
SMC5_009378	00 57 08.105	-72 32 40.18	16.51	51.67	6.94	7.29:		304	**, α CS+ α neb, Fe II dble?
SMC5_011371	00 56 28.170	-72 30 36.80	16.94	41.30	3.81	4.31		502	α CS+ α neb, Fe II?
SMC5_011991	00 55 25.244	-72 29 56.50	16.28	42.03			9.64	182	**, α (CS+neb)
SMC5_012717	00 57 05.450	-72 29 16.20	16.48	39.87	5.66	6.28		316	α CS+ α neb, Fe II?
SMC5_012767	00 55 34.670	-72 29 13.10	16.66	33.56	3.20	3.66		536	k1054, sh, α CS+ α neb, Fe II dble, He I
SMC5_013233	00 56 33.898	-72 28 43.92	18.15	8.09	2.26	2.75:		270	cl, α CS+ α neb, Fe II?
SMC5_013978	00 56 31.140	-72 27 57.80	15.60	50.98			8.08	277	cl, k206, α (CS+neb), Fe II?
SMC5_014052	00 56 23.010	-72 27 53.90	15.35	44.96	10.38	10.07		170	cl, k215, sh, noneb, Fe II
SMC5_014114	00 56 32.261	-72 27 50.17	15.52	40.36			7.20	219	cl, k203, noneb, He I w, Fe II
SMC5_014212	00 54 32.960	-72 27 41.94	15.42	55.28			10.40	227	**, α (CS+neb), Fe II dble
SMC5_014271	00 54 18.116	-72 27 37.21	15.56	46.28	5.27	5.59		388	**, α CS+ α neb, Fe II dble, He I
SMC5_014637	00 56 12.130	-72 27 16.90	15.42	23.33			5.80	182	cl, k242, α (CS+neb)
SMC5_014727	00 56 18.130	-72 27 13.50	15.65	23.72			4.20:	306	cl, k228, α CS+ α neb, Fe II dble?
SMC5_014864	00 56 33.110	-72 27 04.99	16.12	25.09			7.65	146	cl, k419, α (CS+neb), Fe II
SMC5_014878	00 54 59.326	-72 27 02.12	15.71	40.49			5.82	300	**, α (CS+neb), Fe II dble
SMC5_015429	00 55 33.650	-72 26 29.90	17.63	20.97	2.57	2.58		552	k2299, α CS+ α neb
SMC5_015509	00 56 24.620	-72 26 24.70	16.98	44.58			5.43	388	k857, α CS+ α neb
SMC5_015867	00 55 52.279	-72 26 03.77	17.23	31.79			7.45	186	k991, α (CS+neb)
SMC5_016177	00 55 44.521	-72 25 43.91	16.99	30.26			5.85	243	k1017 α CS+ α neb, Fe II dble+w
SMC5_016461	00 55 49.619	-72 25 27.43	14.90	52.33	9.08	9.68		245	k137, bin, sh, **, noneb, Fe II dble, He I
	00 55 49.630	-72 25 27.30	14.90	50.99	8.70	8.99		259	k137, bin, sh, **, noneb, Fe II dble, He I
SMC5_016477	00 56 01.510	-72 25 25.78	18.76	13.74	2.65	2.36		418	α CS+ α neb
SMC5_016486	00 54 46.371	-72 25 22.73	15.58	48.80			5.45	482	**, α (CS+neb), Fe II dble
SMC5_016523	00 55 30.790	-72 25 20.30	15.70	34.46			4.11	406	k278, α CS+ α neb, He I, Fe II
SMC5_016544	00 56 29.100	-72 25 21.50	16.84	44.70	5.69	5.72		365	k837, α CS+ α neb, Fe II dble
SMC5_016824	00 53 44.010	-72 24 56.30	15.06	5.47			1.66	328	α CS+ α neb
SMC5_017596	00 56 33.330	-72 24 19.80	17.16	29.20			7.78	154	k818, α (CS+neb), Fe II?
SMC5_018501	00 56 14.450	-72 23 23.60	15.20	26.46			4.00	331	k128, α CS+ α neb, Fe II dble+w, He I?
SMC5_020211	00 56 06.798	-72 21 35.34	16.86	34.83	4.90	3.63		393	sh, noneb, Fe II dble
SMC5_021152	00 53 12.660	-72 20 29.50	15.30	8.93	1.81	1.94		390	α CS+ α neb
SMC5_021886	00 55 48.566	-72 19 46.88	17.50	19.16	3.21	3.10		388	sh, α CS+ α neb, Fe II dble
SMC5_022295	00 55 14.500	-72 19 18.60	15.92	49.87	?	?			bad pixels in H α , Fe II?
SMC5_022628	00 53 37.080	-72 18 50.60	15.86	22.67			3.39	398	α CS+ α neb, He I asym., Fe II?
SMC5_022842	00 55 49.880	-72 18 42.10	17.77	58.91	8.20:	6.83		318	α CS+ α neb, Fe II dble+w
SMC5_023931	00 56 24.635	-72 17 20.79	17.36	14.59	3.21	3.16		379	sh, α CS+ α neb, Fe II
SMC5_025052	00 55 39.810	-72 16 04.20	17.72	1.43	1.28	1.28		427	Haw, α CS+ α neb
SMC5_025589	00 56 08.450	-72 15 28.00	17.97	16.16	2.90	2.97		347	α CS+ α neb
SMC5_025718	00 54 27.140	-72 15 15.90	16.87	49.15	6.54	5.27		393	sh, noneb, Fe II
SMC5_025816	00 55 16.580	-72 15 04.70	15.62	48.43			8.74	236	α (CS+neb), Fe II
SMC5_025829	00 56 17.880	-72 15 05.90	16.23						no red spectrum, α CS+ α neb
SMC5_026182	00 54 08.940	-72 14 42.50	17.98	23.37			3.94	318	cl, α CS+ α neb

Table 1. continued.

Name	α 2000	δ 2000	Vmag	EW α Å	I(V)	I(R)	Imax	FWHM α km s ⁻¹	Remarks
SMC5_026689	00 54 07.970	-72 14 03.90	17.52	30.79			4.85	335	noneb
SMC5_028368	00 53 11.930	-72 12 04.60	16.61	12.30	2.02	2.03		518	α CS+aneb
SMC5_036967	00 55 40.100	-72 29 44.70	16.36	51.96	8.89	5.31		270	sh, k528, noneb, Fe II dble
SMC5_037013	00 55 13.616	-72 29 13.87	15.50	49.45			9.70	192	**, α (CS+neb), Fe II
SMC5_037137	00 56 26.602	-72 28 09.40	15.84	75.48			10.86	295	cl, k211, noneb, Fe II dble
SMC5_037158	00 55 38.260	-72 27 54.60	17.23	36.97	3.44	3.61		561	k1041, noneb, Fe II?
SMC5_037162	00 54 40.790	-72 27 52.50	16.02	47.38			7.55	261	cl, α (CS+neb), Fe II?
SMC5_038007	00 53 54.170	-72 19 55.42	17.27	13.07	3.15:	2.99:		286	α CS+aneb
SMC5_038312	00 55 18.950	-72 16 56.60	17.72	23.27			4.47	280	α CS+aneb
SMC5_038363	00 55 33.327	-72 16 22.70	16.54	43.73	4.45	5.63		396	sh, noneb, Fe II dble
SMC5_041410	00 54 33.353	-72 32 11.79	16.37	36.90			4.42:	418	**, α CS+aneb, He I, Fe II dble
SMC5_043413	00 55 30.950	-72 29 36.70	15.84	49.29			8.66	229	k27, α (CS+neb)
SMC5_044117	00 56 11.660	-72 28 41.80	16.34	41.62	5.73	5.78		313	cl, k471, α CS+aneb
SMC5_044693	00 56 19.851	-72 28 01.57	15.96	18.33	3.24	3.17		307	cl, k222, α CS+aneb
SMC5_044898	00 56 07.514	-72 27 43.74	16.85	67.52			8.03	345	cl, k480, α (CS+neb), Fe II dble
SMC5_045353	00 54 22.312	-72 27 07.72	15.53	55.51	6.88	6.35		356	sh, **, noneb, Fe II dble
SMC5_045747	00 55 40.150	-72 26 41.70	16.58	42.39			6.52	288	k529, α (CS+neb), Fe II?
SMC5_046388	00 53 26.980	-72 25 41.40	16.47	3.50	1.4	1.3		412	Haw, α CS+aneb
SMC5_046462	00 56 22.590	-72 25 47.20	16.76	32.52	4.88	4.28		334	k874, α CS+aneb
SMC5_047763	00 55 42.620	-72 23 58.20	16.04	10.60			3.20	406	k522, α CS+aneb
SMC5_048045	00 55 56.320	-72 23 33.30	16.59	44.47			6.51	306	k509, α (CS+neb)
SMC5_048047	00 57 30.565	-72 23 32.73	15.90	31.78	5.35	4.82:		300	**, α CS+aneb, Fe II?
SMC5_048289	00 53 50.650	-72 23 09.20	15.87	18.71	3.79	3.33		266	α CS+aneb
SMC5_049651	00 56 19.491	-72 21 17.05	17.86	3.95	1.72	1.61		370	cl, α CS+aneb
SMC5_049746	00 54 04.690	-72 21 06.30	16.49	43.13			6.58	245	α (CS+neb)
SMC5_049780	00 55 13.492	-72 21 06.75	16.71	43.19	5.26	5.18		393	α CS+aneb, Fe II dble, He I dble?
SMC5_049996	00 53 10.350	-72 20 42.30	15.88	36.69	4.43	4.01		409	α CS+aneb, Fe II dble
SMC5_051315	00 54 04.820	-72 18 50.70	17.96	3.81	1.86	1.71		336	α CS+aneb
SMC5_052688	00 55 47.140	-72 16 34.00	15.49	0.10	1.37	1.23		175	α CS+aneb
SMC5_053267	00 55 50.490	-72 15 39.90	17.04	33.52	4.96	4.76		338	α CS+aneb, Fe II
SMC5_053756	00 54 12.372	-72 14 48.00	16.53	34.17			8.88	161	cl, α (CS+neb), Fe II dble
SMC5_055592	00 53 22.720	-72 11 55.70	16.68	43.56			10.51	173	cl, α CS+aneb, Fe II
SMC5_061950	00 56 29.960	-72 14 41.70	17.67	2.04	1.39	1.33		431	α CS+aneb
SMC5_064327	00 56 14.900	-72 28 47.50	15.41	67.91	7.86	7.92		350	cl, k238, α CS+aneb, Fe II dble
SMC5_064576	00 54 46.290	-72 28 05.00	17.38	31.25			6.77:	211	cl, α CS+aneb
SMC5_064745	00 54 28.887	-72 27 38.20	15.69	24.74	3.75	2.80		377	**, α CS+aneb, He I complex
SMC5_064832	00 54 54.577	-72 27 23.64	16.79	38.44			6.07	300	α (CS+neb)
SMC5_065055	00 53 55.340	-72 26 45.30	14.72	24.23	3.47	3.22		390	α CS+aneb, He I dble
SMC5_065746	00 54 01.887	-72 24 45.57	17.42	30.76	3.65	3.77		413	α CS+aneb
SMC5_066754	00 55 21.820	-72 21 33.70	16.09	36.90			8.85	172	α (CS+neb)
SMC5_067333	00 56 51.700	-72 19 45.20	16.21	14.75	2.52	2.49		393	α CS+aneb, He I
SMC5_073581	00 56 26.600	-72 26 23.00	16.22	13.81	2.45	2.65		365	α CS+aneb
SMC5_073594	00 53 21.410	-72 26 08.90	16.13	12.51	3.20	2.98		227	α CS+aneb
SMC5_074402	00 53 04.530	-72 20 49.30	15.83	35.22			4.90	331	α (CS+neb), He I?, Fe II?
SMC5_074471	00 53 26.610	-72 20 18.60	14.97	19.08	3.19	3.12		330	α CS+aneb
SMC5_075061	00 56 30.580	-72 16 16.20	17.58	13.18			4.83	141	α (CS+neb)
SMC5_075360	00 54 05.990	-72 13 51.60	15.78	57.33	6.27	5.86		418	sh, noneb, Fe II dble
SMC5_078338	00 56 25.450	-72 27 07.00	15.49	49.32	11.99	10.68		152	cl, sh, k213, noneb, Fe II
SMC5_078440	00 56 50.560	-72 15 07.30	15.63	12.23	2.34	1.89		409	α CS+aneb, Fe II dble?
SMC5_078928	00 57 09.690	-72 26 57.50	17.48	57.96	6.97	4.03		322	sh, α CS+aneb, Fe II strong, He I
SMC5_080910	00 54 24.272	-72 13 49.41	16.74	33.25	4.19	3.80		436	sh, noneb, Fe II dble
SMC5_081260	00 54 13.120	-72 14 35.60	17.77	1.80	1.14	1.15		497	cl, Haw, α CS+aneb
SMC5_082042	00 56 18.260	-72 17 46.80	16.39	65.27			7.40	384	α CS+aneb, Fe II dble+w
SMC5_082202	00 57 30.310	-72 15 58.40	15.76	30.55	4.35	4.44		350	cl, sh, noneb, Fe II?
SMC5_082543	00 56 54.005	-72 28 50.18	17.05	50.70			7.32	313	k754, α (CS+neb)
SMC5_082819	00 56 07.190	-72 28 13.70	13.46	11.88			2.68	286	cl, sh, α (CS+neb), Fe II
SMC5_082941	00 53 53.660	-72 22 01.40	15.75	59.43	7.33	6.15		368	α CS+aneb, Fe II dble
SMC5_083491	00 53 19.930	-72 22 29.20	15.95	13.37	2.29	1.71		456	α CS+aneb
SMC5_085503	00 54 47.457	-72 27 58.77	16.88	21.79	2.79	4.89		284	cl, sh, α CS+aneb, Fe II
SMC5_086200	00 55 32.480	-72 27 52.00	17.29	12.79				622	k1062, α CS+aneb
SMC5_086251	00 55 35.310	-72 15 11.70	16.86	25.47	3.00	3.05		529	sh, α CS+aneb
SMC5_086581	00 55 55.498	-72 26 58.34	17.53	25.07	4.17	4.36		325	k2118, α CS+aneb
SMC5_086890	00 56 16.439	-72 27 56.38	16.88	50.96			7.16	316	cl, k462, α (CS+neb), Fe II dble
SMC5_086983	00 56 20.410	-72 28 06.40	16.24	33.07			4.45	350	cl, k441, α (CS+neb), Fe II dble
SMC5_087004	00 56 21.394	-72 27 27.89	17.18	44.24	6.07	5.90		336	cl, k882, α CS+aneb, Fe II dble
SMC5_090914	00 56 20.250	-72 27 28.70	16.03	42.42			7.23	261	cl, k442, α (CS+neb)
SMC5_190576	00 56 44.310	-72 29 06.30	14.56	26.74			5.78	222	α (CS+neb), He I dble
SMC5_002807	00 56 09.420	-72 28 09.30	14.62	20.7	3.00	4.07		374	cl, bin, cool Sg, k44
SMC5_037102	00 56 06.450	-72 28 27.70	17.32	360	41.84	33.29		337	cl, HB[e], k485
SMC5_081994	00 56 30.750	-72 27 02.00	17.32	673			2019	64	cl, PNe, k4154

Table 6. Lines identification of SMC5_037102. E=Emission, A=Absorption, sh=shell component of Balmer lines.

Wave. (Å)	ID	E/A
3972.63	sh He 3970.074	A
3994.70	[Cr II] (4F) 3992.080	E
4026.84	Fe II (127) 4024.552	E
4028.45	[Ni II] (4F) 4025.800	E
4030.34	He I (3) 4026.190	A
4056.15	O II (50,98) 4054.100	A
4062.82	O II (97) 4060.580	A
4070.81	[S II] (1NF) 4068.620	E
4104.56	sh Hδ 4101.737	A
4119.16	[Ti II] (20F) 4116.600	E
4134.11	[Fe II] (24F) 4131.510	E
4175.74	Fe II (27) 4173.450	E
4179.32	[Fe II] (21F) 4177.210	E
4180.66	[Fe II] (23F)+ Fe II (28) 4178.855	E
4187.10	O II (36) 4185.456	A
4207.78	Fe II (P22) 4205.480	E
4229.76	Al II (46) 4226.827	A
4232.35	? [Fe IV] (1F) 4229.800	E
4235.39	Fe II (27) 4233.170	E
4236.86	[Fe II] (37F) 4234.810	E
4246.49	[Fe II] (21F) 4243.980	E
4271.75	? S II (49) 4269.760	A
4279.30	O II (54,67) 4277.050	E
4289.76	[Fe II] (7F) 4287.400	E
4298.16	Fe II (28) 4296.567	E
4302.16	Ti II (41) 4300.052	E
4305.25	Fe II (27) 4303.166	E
4321.86	[Fe II] (21F) 4319.620	E
4343.38	sh Hγ 4340.470	A
4349.01	[Fe II] (21F) 4346.850	E
4354.75	Fe II (27) 4351.640	E
4360.75	[Fe II] (21,6F) 4358.230	E
4361.78	[Fe II] (7F) 4359.340	E
4385.58	[Fe II] (6F) 4382.750	E
4390.62	He I (51) 4387.930	A
4416.11	[Fe II] (6F) 4414.450	E
4418.64	[Fe II] (6F) 4416.270	E
4419.65	? Fe II (27) 4416.817	E
4445.29	? Ti II (19) 4443.802	E
4454.54	[Fe II] (7F) 4452.110	E
4460.43	[Fe II] (6F) 4457.950	E
4468.93	[Ni II] (10F) 4466.330	E
4472.66	[Fe II] (6F) 4470.290	E
4475.51	He I (14) 4471.477	A
4477.64	[Fe II] (7F) 4474.910	E
4479.59	O II (88) 4477.880	A
4491.19	[Fe II] (6F)+Fe II (37) 4489.465	E
4493.51	Fe II (37) 4491.401	E
4510.51	Fe II (38) 4508.280	E
4517.45	[Fe II] (6F)+ Fe II (37) 4515.118	E
4523.19	Fe II (37) 4520.225	E
4525.15	Fe II (38) 4522.630	E
4527.05	Ti II (60) 4524.732	E
4550.54	[Fe I] (21F) 4548.320	E
4551.81	Fe II (38) 4549.467	E
4558.07	Fe II (37) 4555.890	E
6459.66	Fe II (74) 6456.380	E
6462.01	?? Fe III (3P) 6458.680	E
6494.99	Fe II 6491.280	E
6496.59	Fe II 6493.050	E
6519.07	Fe II (40) 6516.050	E
6521.43	Fe II 6517.010	E
6566.60	sh Hα 6562.817	E
6685.45	He I (45) 6678.149	A
6720.12	[S II] (2F) 6717.000	E
6733.21	[Fe II] (31F) 6729.850	E
6734.50	[S II] (2F) 6731.300	E
7159.16	[Fe II] (14F) 7155.140	E

Table 7. Lines identification for SMC5_081994. E=Emission, A=Absorption, Neb.=nebular, sat=satellite emission line. The flux was measured above the continuum with an accuracy of 20%.

Wave. (Å)	ID	flux (Å)	comment
3966.78	He I (5) 3964.44	3.97	E
3969.50	[Ne III] Neb (1F) 3967.51	62.47	E
3972.12	He I 3970.074	47.01	E
4010.62	[Fe III] (4F) 4008.30	0.61	E
4011.51	He I (55) 4009.27	0.72	E
4028.29	He I (3) 4026.60 + He I (18) 4026.36	6.81	E
4061.58	[F IV] (1F) 4059.30	0.15	E
4070.84	[S II] Neb (1F) 4068.62	9.94	E
4073.74	O II (49) 4071.20	1.87	E
4078.61	[S II] Neb (1F) 4076.22	3.14	E
4099.54	O II (20,48) 4097.26	1.93	E
4102.37	He I (3) 4100.04 + Hδ sat	1.82	E
4103.98	Hδ 4101.74	58.94	E
4105.25	Hδ sat	1.68	E
4116.73	[Fe II] (23F) 4114.48	0.50	E
4123.11	He I (16) 4120.89 + He I (16) 4120.81 + S II (2) 4121.0	1.15	E
4130.77	?Fe II (27) 4128.73	0.39	E
4132.42	O II (19) 4129.34 + Si II (3) 4128.05		A
4145.95	He I (53) 4143.76 + O II (106) 4143.52+4143.77	2.78	E
4183.42	N II (49) 4181.17+4182.42	1.22	E
4191.89	O II (36) 4189.79	0.34	E
4202.12	He I (3) 4199.83	3.09	E
4229.79	[Fe V] (2F) 4227.44	9.63	E
4246.40	[Fe II] (21F) 4243.98	1.34	E
4247.27	[Fe II] (21F) 4244.81	0.28	E
4279.09	O II (54, 67) 4276.71	1.00	E
4289.73	[Fe II] (7F) 4287.40	1.74	E
4308.47	[Fe II] (21F) 4305.90	0.26	E
4322.08	[Fe II] (21F) 4319.62	0.32	E
4328.72	[Ni II] (3F) 4326.85	0.34	E
4341.07	He II (3) 4338.67+ Hγ sat	4.54	E
4342.81	Hγ 4340.47	148.64	E
4344.37	Hγ sat		E
4349.39	O II (16) 4347.42 or [Fe II] (36F) 4347.35	0.33	E
4355.18	[Fe II] (21F) 4352.78	0.58	E
4361.66	[Fe II] (7F) 4359.34	1.66	E
4363.86	[O III] Neb sat		E
4365.55	[O III] Neb (2F) 4363.21	76.57	E
4367.04	[O III] Neb sat		E
4390.34	He I (51) 4387.93	2.21	E
4411.74	[Fe II] (22F) 4407.25+4410.75	0.36	E
4416.15	[Fe II] (7F) 4413.78	0.88	E
4418.69	[Fe II] (6F) 4416.27	1.19	E
4439.84	He I (50) 4437.55 + Mg II (19) 4436.48	0.68	E
4454.54	O II (5) 4452.38	0.37	E
4460.54	[Fe II] (6F) 4457.95	0.45	E
4474.94	He I (14) 4471.47	19.84	E
4477.25	O III (37) 4474.95		E
4544.08	He II (2) 4541.59 + Fe II (38) 4541.52	4.95	E
6530.78	[N II] (1F) 6527.40	2.41	E
6551.69	[N II] Neb (1F) 6548.06	350.90	E
6563.73	He II (2) 6560.10 + Hα sat	91.99	E
6566.43	Hα 6562.82	2943.0	E
6570.12	Hα sat	15.6	E
6583.66	[N II] Neb sat	4.82	E
6587.11	[N II] Neb (1F) 6583.37	1167.0	E
6590.62	[N II] Neb sat	6.14	E
6681.80	He I (46) 6678.15	50.62	E
6686.88	He II (7) 6683.39	3.78	E
6704.58	[Fe II] (43F) 6700.68 + [Ni II] (8F) 6700.61	0.18	E
6713.17	[S II] Neb sat	1.00	E
6720.17	[S II] Neb (2F) 6716.42	28.35	E
6734.56	[S II] Neb (2F) 6730.78	52.87	E
6737.93	[S II] Neb sat	1.85	E
6895.00	He II (7) 6890.88	5.37	E
7009.46	[Ar V] (1F) 7005.70	28.43	E
7055.02	[Fe II] (17F) 7051.04		E
7065.41	He I sat		E
7069.11	He I (10) 7065.28	141.50	E
7073.16	He I sat	0.79	E
7139.84	[Ar III] (1F) 7135.78	29.52	E
7159.23	[Fe II] (14F) 7155.14	4.01	E

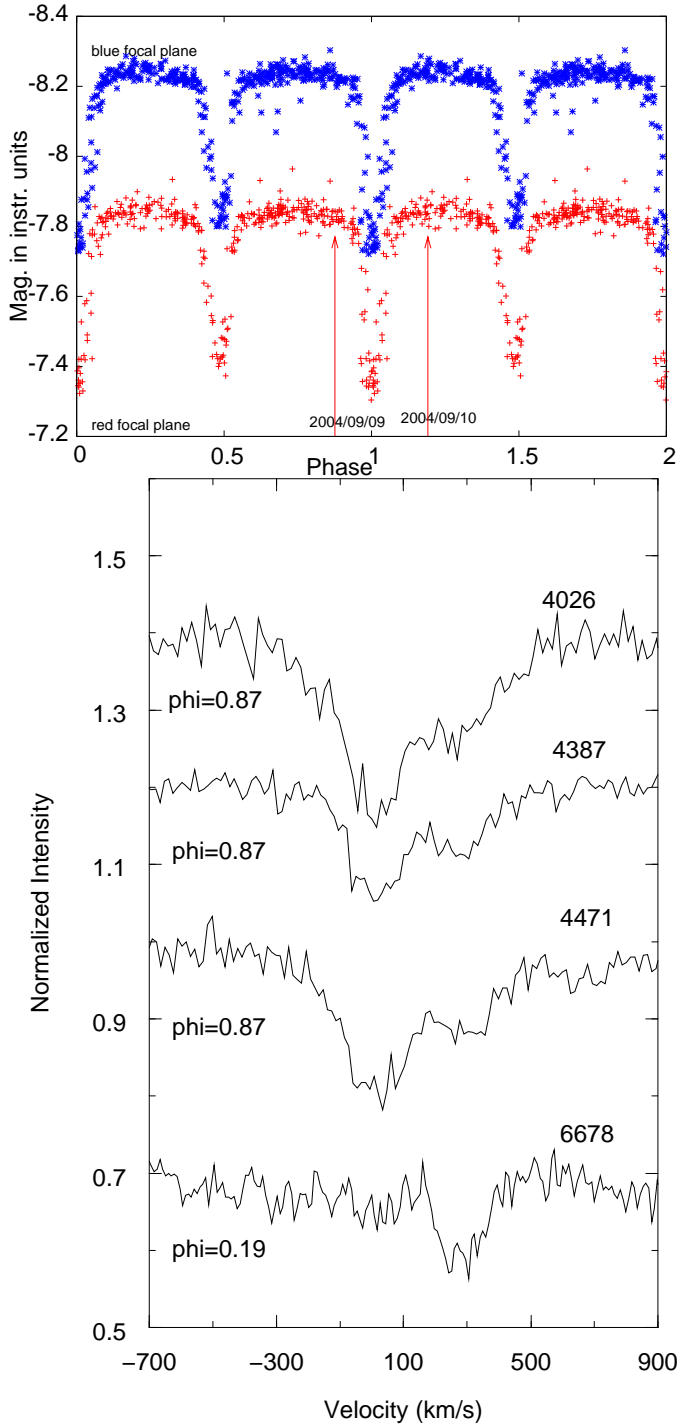


Fig. 5. SMC5_000977. Top: light curve folded in phase with $P=3.128$ d. Bottom: Helium lines taken at $\phi=0.87$ for the blue ones and at $\phi=0.19$ for the red one.

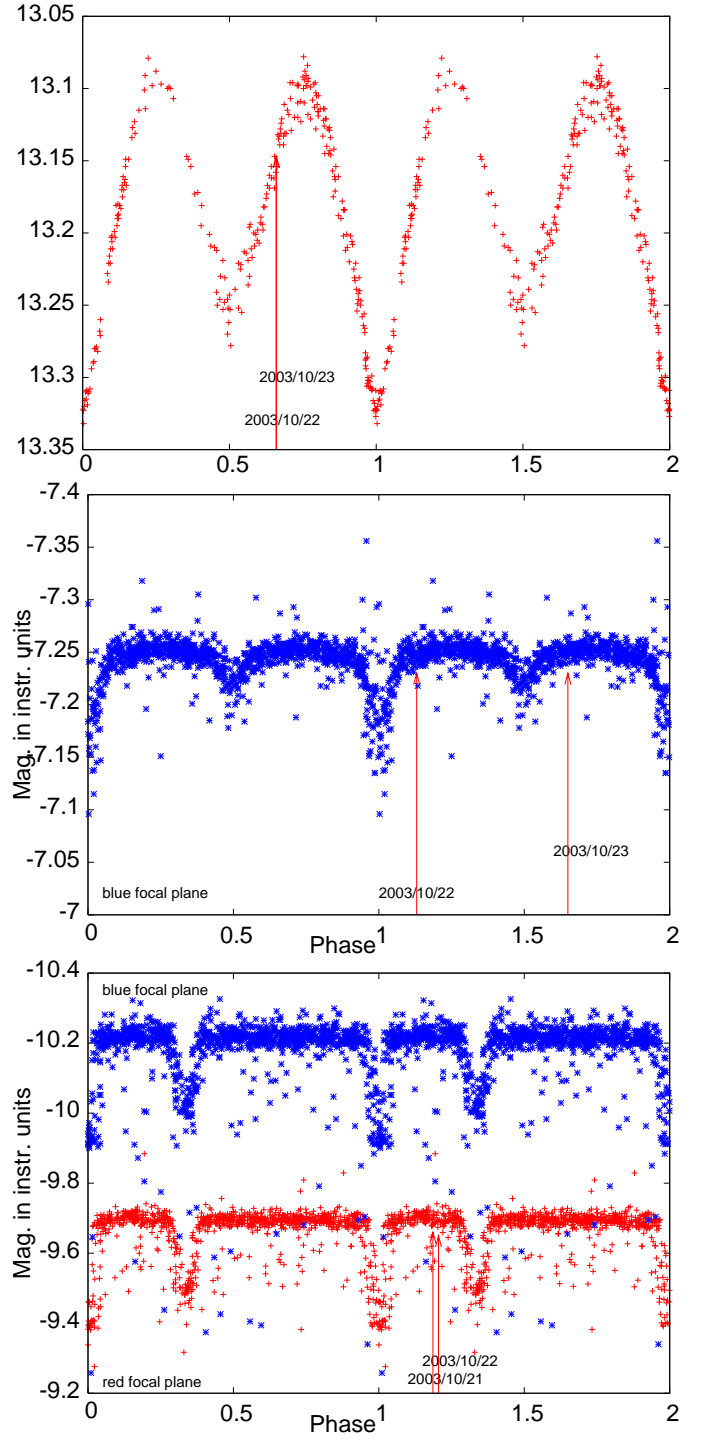


Fig. 6. Top: SMC5_002807 folded in phase with $P=454.959$ d (OGLE data, Imag). Middle: SMC5_003789 Be star folded in phase with $P=2.087$ d (MACHO data). Bottom: SMC5_0004477 folded in phase with $P=4.480$ d (MACHO data).

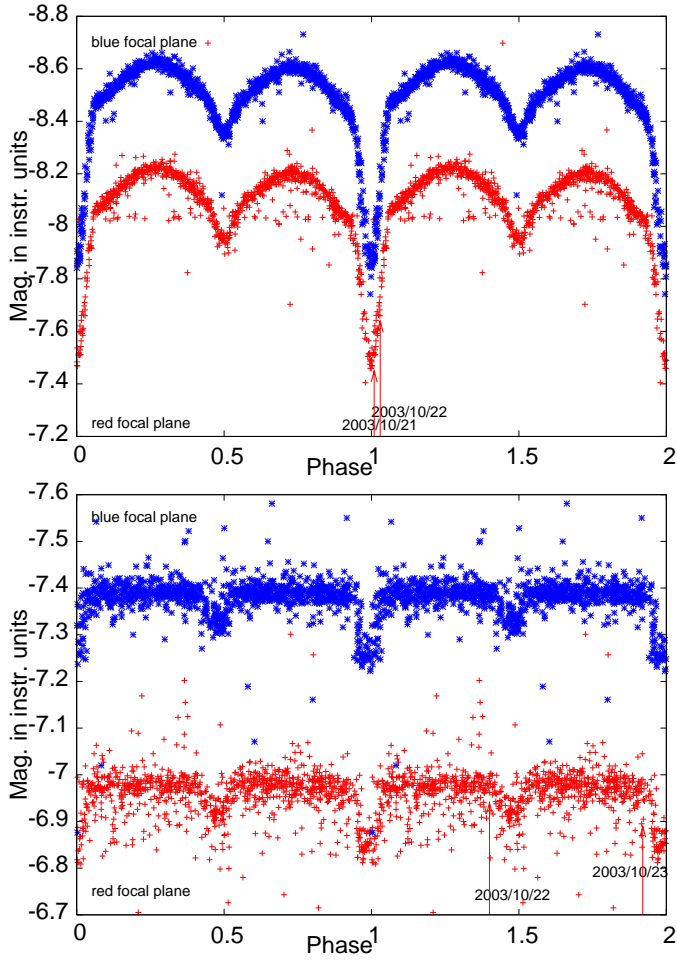


Fig. 7. Top: SMC5_004534 folded in phase with $P=4.051$ d. Bottom: SMC5_013723 folded in phase with $P=2.059$ d.

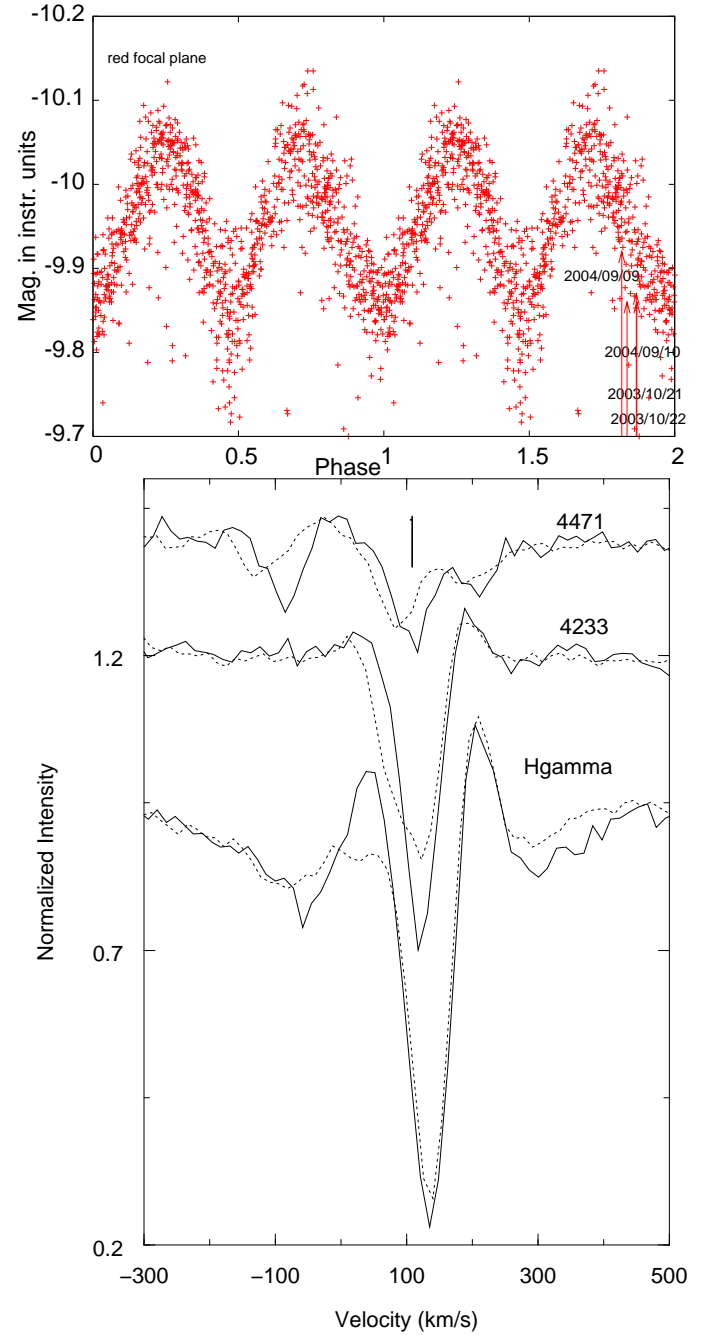


Fig. 8. SMC5_016461. Top: light curve folded in phase with $P=54.337$ d. Bottom: Lines of He I 4471, Fe II 4233 and H γ for the spectra obtained in 2003 (full line) at $\phi=0.89$ and in 2004 (dotted line) at $\phi=0.82$ just before a primary eclipse

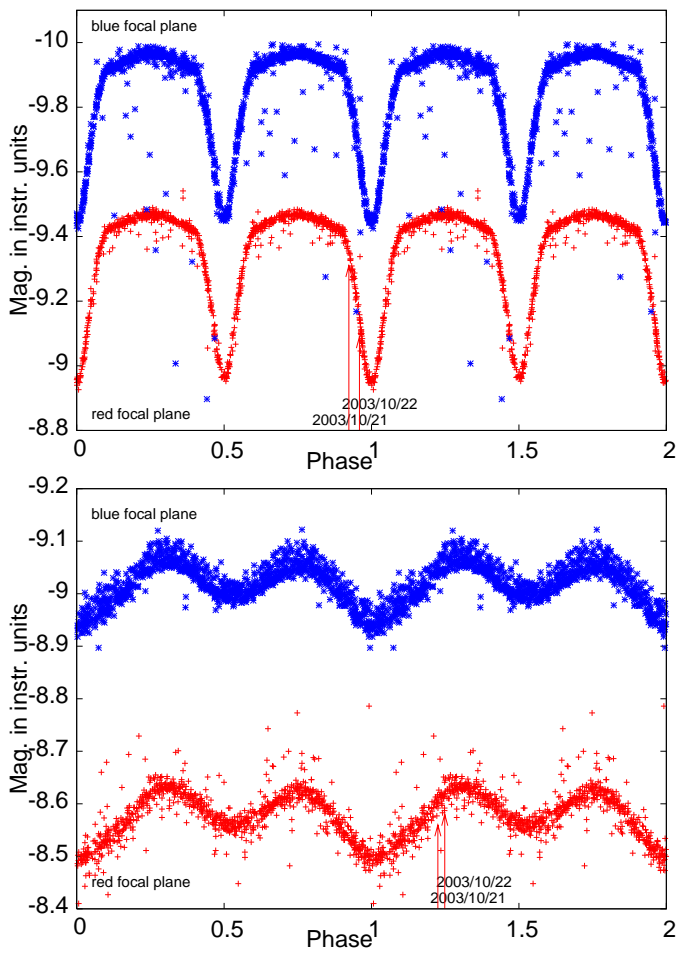


Fig. 9. Top: SMC5_020391 folded in phase with $P=2.320$ d. Bottom: SMC5_023571 folded in phase with $P=3.534$ d.

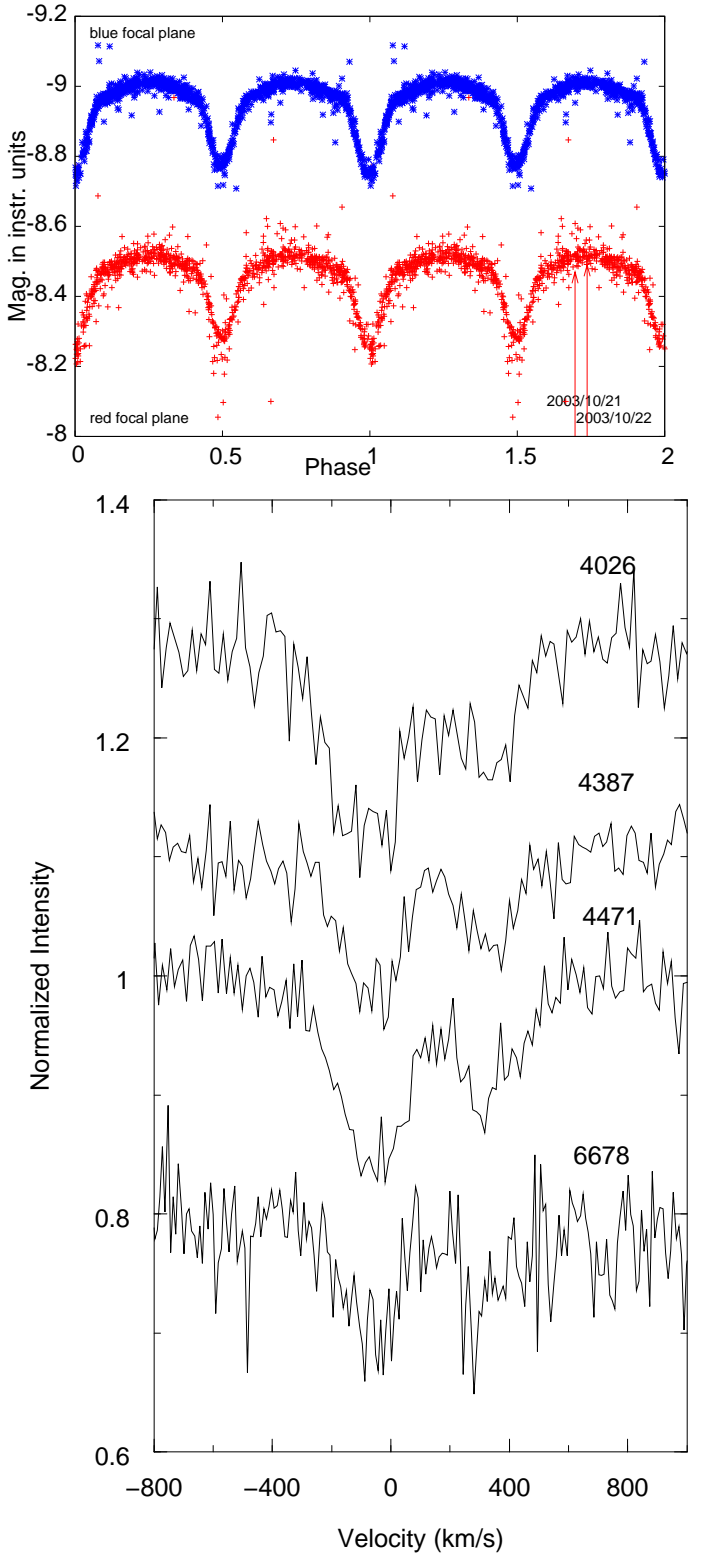


Fig. 10. SMC5_023641. Top: light curve folded in phase with $P=2.010$ d. Bottom: Helium lines taken at $\phi=0.70$ for the blue ones and at $\phi=0.74$ for the red one.

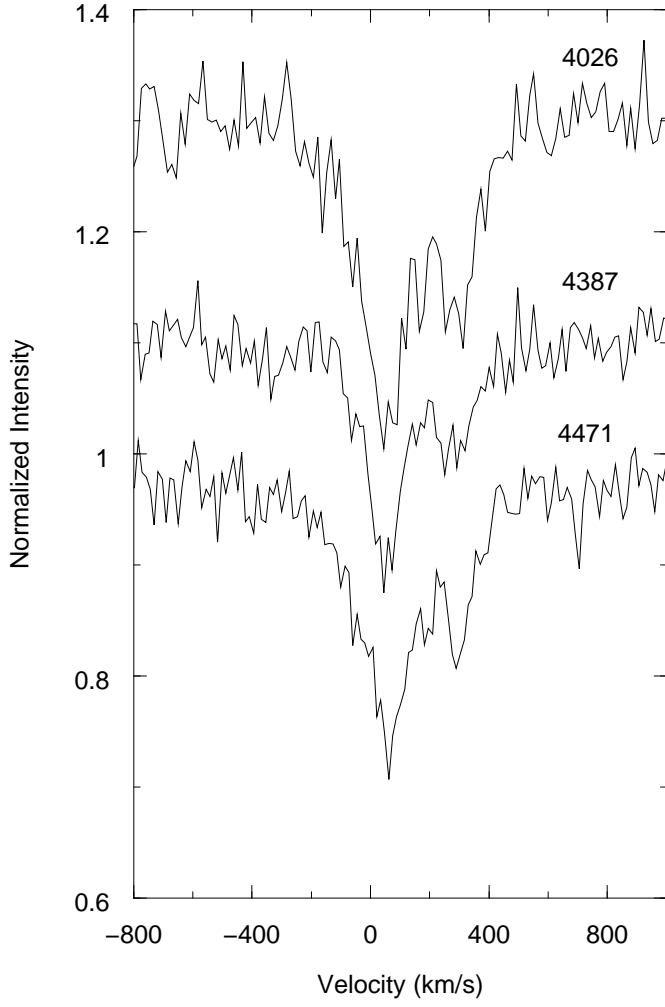


Fig. 11. Blue helium lines of SMC5_052663

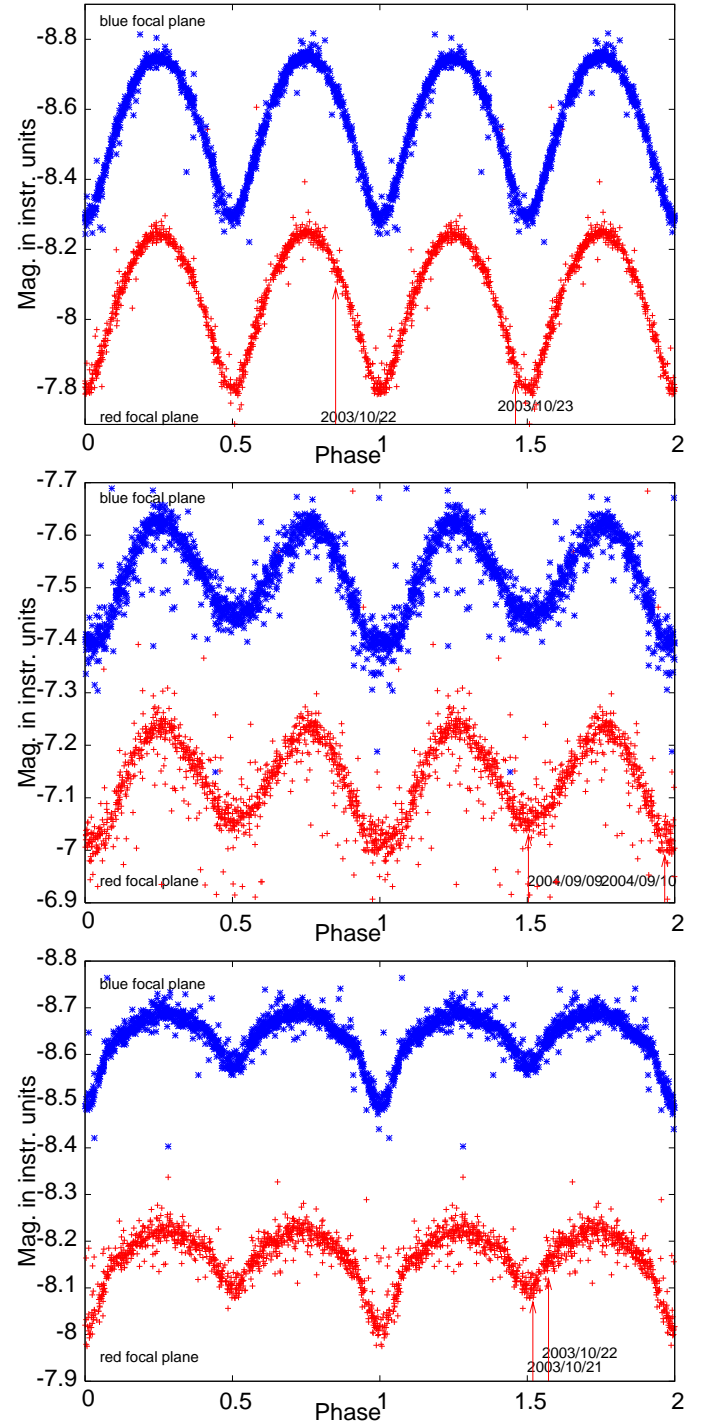


Fig. 12. Top: SMC5_049816 folded in phase with $P=0.664$ d. Middle: SMC5_074928 folded in phase with $P=2.137$ d. Bottom: SMC5_084353 folded in phase with $P=1.557$ d.

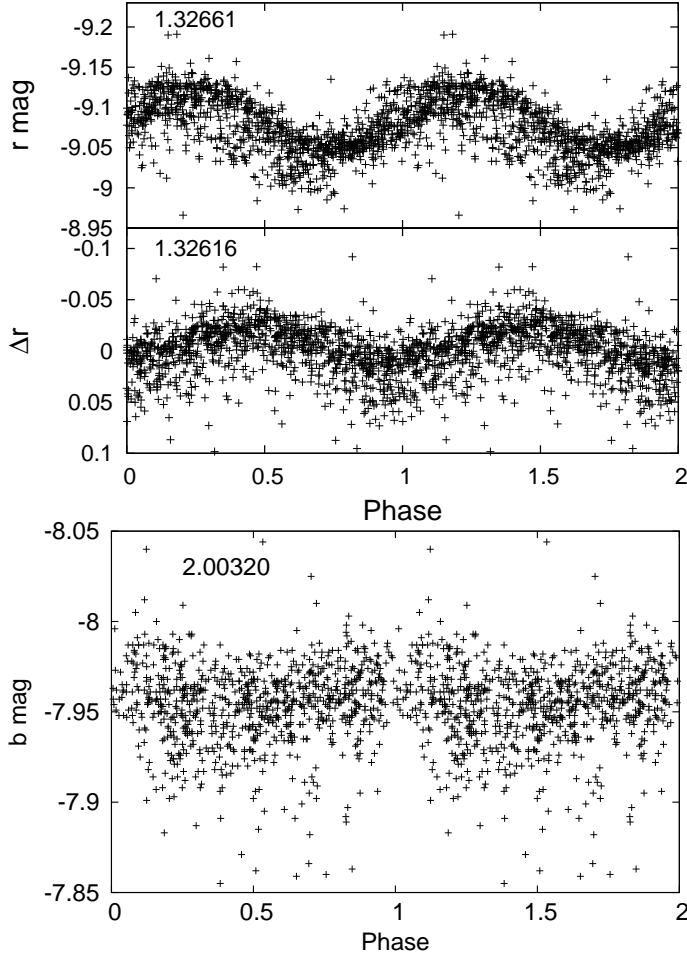


Fig. 13. Be SMC5_2232 folded in phase: top with $f_1=1.32661\text{c d}^{-1}$, middle with $f_2=1.32616\text{c d}^{-1}$ after prewhitening for f_1 . Bottom: Be SMC5_3296 folded in phase with $f=2.00320\text{c d}^{-1}$

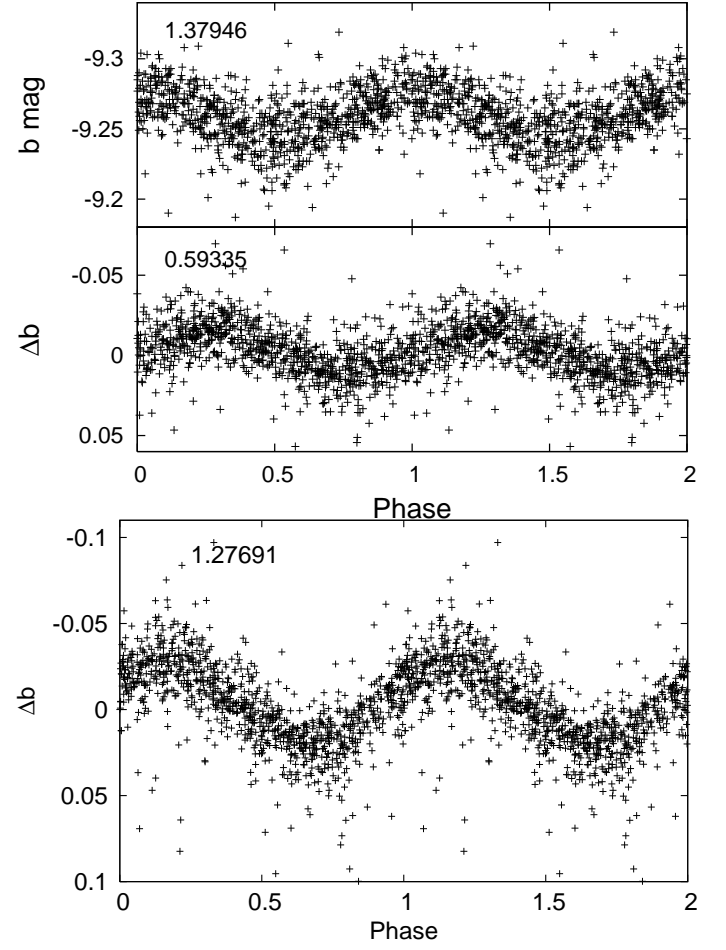


Fig. 14. Be SMC5_13978 folded in phase: top with $f_1=1.37946\text{c d}^{-1}$, middle with $f_2=0.59335\text{c d}^{-1}$ after prewhitening for f_1 . Bottom: Be SMC5_14212 folded in phase with $f=1.27691\text{c d}^{-1}$.

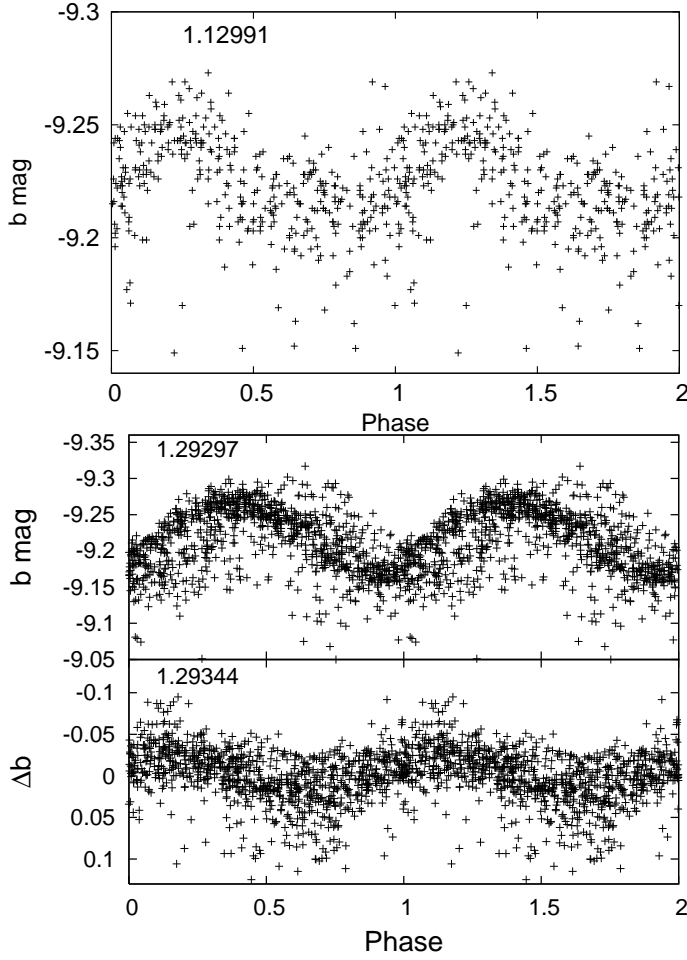


Fig. 15. Top: Be SMC5_14727 folded in phase with $f=1.12991 \text{ c d}^{-1}$. Be SMC5_16523 folded in phase: middle with $f_1=1.29297 \text{ c d}^{-1}$, bottom with $f_2=1.29344 \text{ c d}^{-1}$ after prewhitening for f_1 .

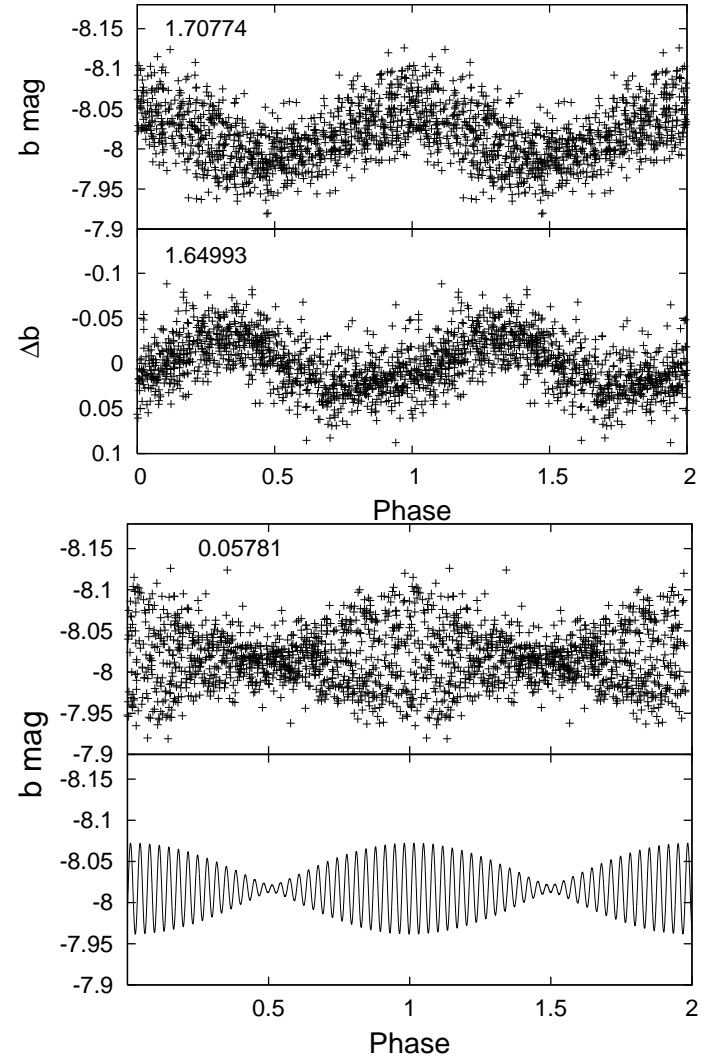


Fig. 16. Be SMC5_16544 folded in phase: top with $f_1=1.70774 \text{ c d}^{-1}$, middle up with $f_2=1.64993 \text{ c d}^{-1}$ after prewhitening for f_1 . Be SMC5_16544 beating diagram, middle down: light-curve folded with the beating frequency 0.05781 c d^{-1} ; bottom: sum of the 2 sinusoidal functions.

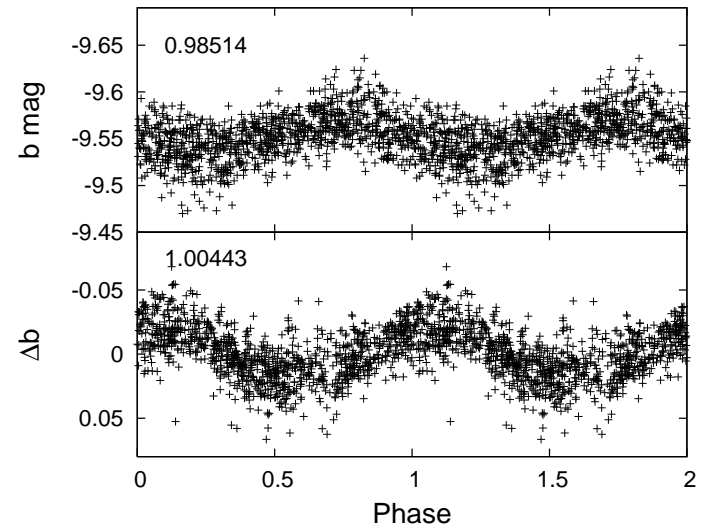


Fig. 17. Be SMC5_21152 folded in phase: middle down with $f_1=0.98514 \text{ c d}^{-1}$, bottom with $f_2=1.00443 \text{ c d}^{-1}$ after prewhitening for f_1 .

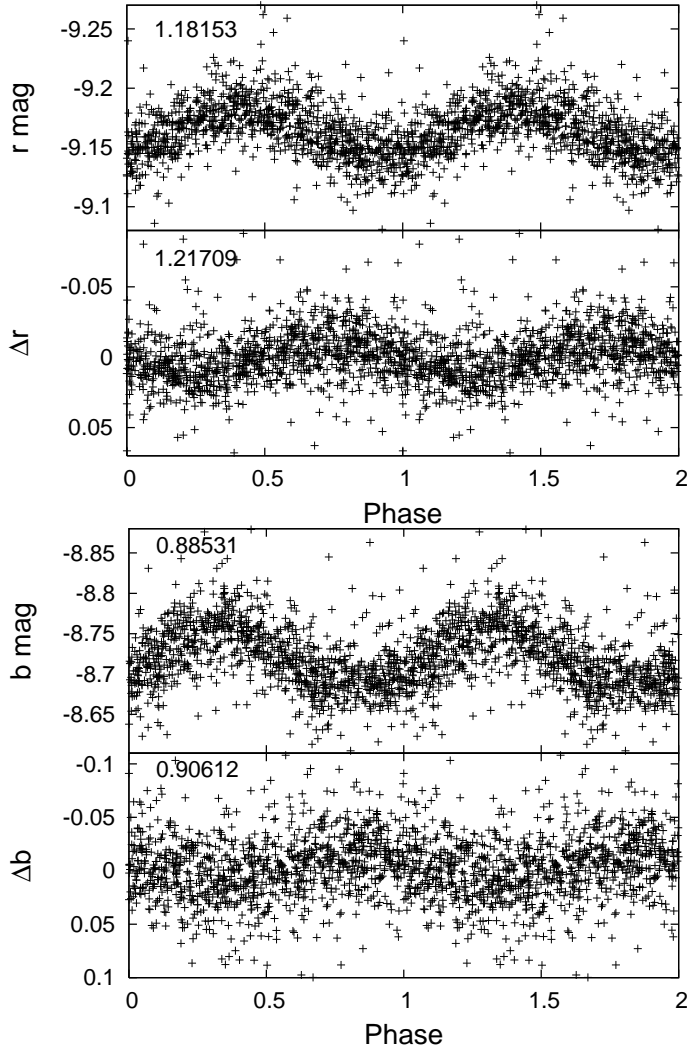


Fig. 18. Be SMC5_37013 folded in phase: top with $f1=1.18153\text{c d}^{-1}$, middle up with $f2=1.21709\text{c d}^{-1}$ after prewhitening for $f1$. Be SMC5_37162 folded in phase: middle down with $f1=0.88531\text{c d}^{-1}$, bottom with $f2=0.90612\text{c d}^{-1}$ after prewhitening for $f1$.

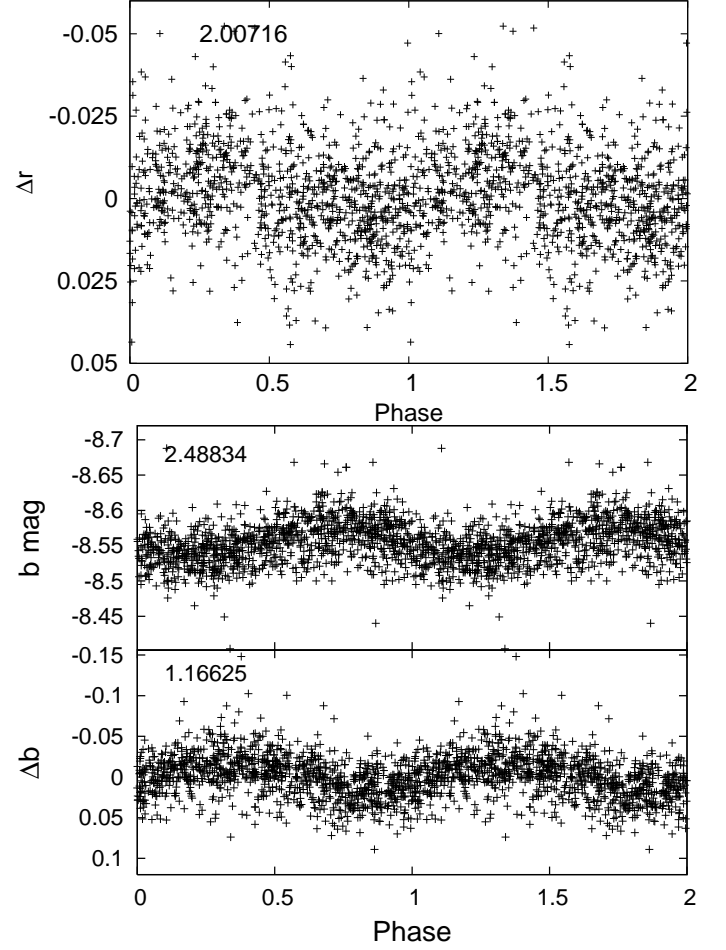


Fig. 19. Top: Be SMC5_43413 folded in phase with $f=2.00716\text{c d}^{-1}$. Be SMC5_82042 folded in phase: middle with $f1=2.48834\text{c d}^{-1}$, bottom with $f2=1.16625\text{c d}^{-1}$ after prewhitening for $f1$.

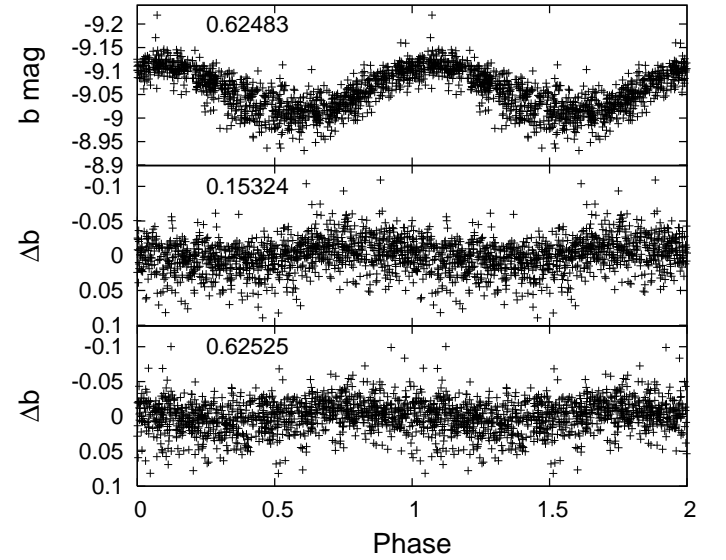


Fig. 20. Be SMC5_82941 folded in phase: top with $f1=0.62483\text{c d}^{-1}$, middle with $f3=0.15324\text{c d}^{-1}$ after prewhitening for $f1$, and bottom with $f2=0.62525\text{c d}^{-1}$ after prewhitening for $f1$ and $f2$.

